Wave scattering by a vertical cylinder with a submerged porous plate: Further analysis

Yang Li[1], Xuanlie Zhao[1]*, Jing Geng[1], Edward Mackay[2], Lars Johanning[1,2]

1. *College of Shipbuilding Engineering, Harbin Engineering University, Harbin, 150001, China*
2. *College of Engineering, Mathematics and Physical Sciences, Exeter University, Cornwall TR10 9FE, UK*

* Corresponding author

Abstract

In this paper, based on linear potential flow theory, an alternative semi-analytical model is developed using the potential decomposition method for wave interaction with a vertical cylinder with a submerged porous plate. The semi-analytical model is verified by comparing with the previous analytical results and the numerical results. The influence of geometrical/physical parameters is further investigated. Results show that there exists a critical frequency beyond which the wave loads on the vertical cylinder are mitigated significantly. The submergence and the radius of the porous plate are the key factors affect the wave loads on the cylinder.

Keywords: Wave loads mitigation; Porous plate; Semi-analytical model; Critical frequency.

1. Introduction

Due to the simplicity in manufacturing and installation, pile-type foundations are often used in coastal and offshore engineering, such as offshore wind turbines, seaports, offshore platforms. (Dhanak and Xiros, 2016). Mitigating the wave loads on the pile is beneficial for lowering its construction cost. Since porous structures dissipate wave energy, it is widely used in coastal engineering (Takahashi et al., 2003; Huang et al., 2011; Liu and Li, 2013; Mackay and Johanning, 2020; Zhai et al., 2021; Zheng et al., 2020). Meanwhile, porous structures are also expected to protect the offshore structures from heavy loads triggered by sea waves (Sun and Jahangiri, 2017).

Many investigations have been carried out to investigate the effect of porous structures on wave loads acting on coastal and offshore structures. Kaligatla et al. (2017) found that the existence of the porous wall is beneficial for mitigation of the wave loads on the seawall. Koley and Sahoo (2021) investigated water wave interaction with an array of vertical flexible porous barriers. Occurrences of Bragg resonance and cloaking of the multiple barriers were analyzed. Chanda and Nandan Bora (2020; 2022) carried out the analytical investigation on the surface and flexural gravity waves interaction with a pair of submerged vertical porous barriers above a porous seabed. Compared with that of water waves, the incorporation of the flexural gravitational waves leads to different hydrodynamic problems.

Williams et al. (2000) theoretically studied the wave diffraction from a floating cylinder whose middle part is porous and found that the porous portion affects the wave forces significantly. Teng et al. (2000; 2001), Sun et al. (2005), Ning et al. (2017), Liang et al. (2020), and Mackay et al. (2019; 2021) investigated hydrodynamic characteristics of the cylinder with porous sidewall. They found that the wave loads on the inner cylinder can be effectively reduced by properly designing the upper porous wall. Sarkar and Bora (2019; 2020) found that the porous medium located at the lower part of the cylinder also leads to the reduction of the wave loads on the cylinder. Liu et al. (2018) and Behera et al. (2020) analyzed the effect of the multiple porous barriers on the wave loads on the inner cylinder. It was found that the hydrodynamic forces on the inner cylinder are reduced significantly as the number of porous barriers increased. Wu and Chwang (2002) examined the impact of a porous plate on wave loads on a vertical cylinder. They found that the horizontal porous plate is of interest from the point of view of wave loads reduction.

We note that the analytical solution presented in Wu and Chwang (2002) requires the solution of the complex dispersion relationship caused by the horizontal plate. Based on linear potential flow theory, Liu et al. (2011) developed a new semi-analytical model for the submerged porous disk. The advantage of the method in Liu et al. (2011) is that there is no requirement for solving the complex dispersion relationship. Liu et al. (2011) formulated the radial eigenfunction in a circular fluid region based on the potential decomposition method. Mathematically, an eigenfunction decomposition for the problem of a cylinder with a ring-shaped porous submerged plate has not yet been presented.

Triggered by the investigation of Wu and Chwang (2002) and Liu et al. (2011), in the present work, we aim at developing an alternative semi-analytical solution by avoiding the solution of the complex dispersion relationship (see Eq. (18) in Ref. (Chwang and Wu, 1994).). This research will extend the analytical solutions for wave interaction with the conventional structure of a vertical cylinder equipped with a submerged porous plate. Besides, the contribution of this paper is to explore the underlying physical mechanism of wave loads variations of the vertical cylinder with the submerged porous plate, as well as the influence of geometrical/physical parameters.

This paper is organized as follows. In Section 2, problem definition and semi-analytical solution are described. In Section 3, numerical results and discussions are presented. Finally, concluding remarks are given in Section 4.

2. Problem definition and semi-analytical solution

2.1 The boundary value problem

The problem of wave scattering by a vertical cylinder with a submerged horizontal porous plate is considered here (shown in Fig. 1). The structure is subjected to regular waves propagating along the negative x-direction with wave height H ($H = 2A$, where A is wave amplitude) and angular frequency ω. Symbolically, a, b, h_1, h_2, and d represent the outer plate radius, the cylinder radius, the draft of the porous plate, the distance between the plate and the seabed, and the water depth, respectively. The cylindrical polar coordinate (r, θ, z) with its origin O located at the center of the cylinder on the still-water level is used to define the mathematical problem.

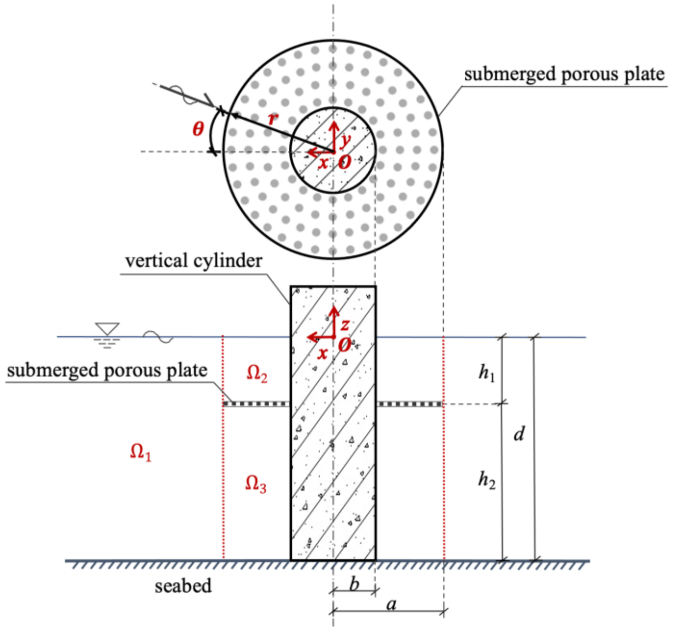

a)

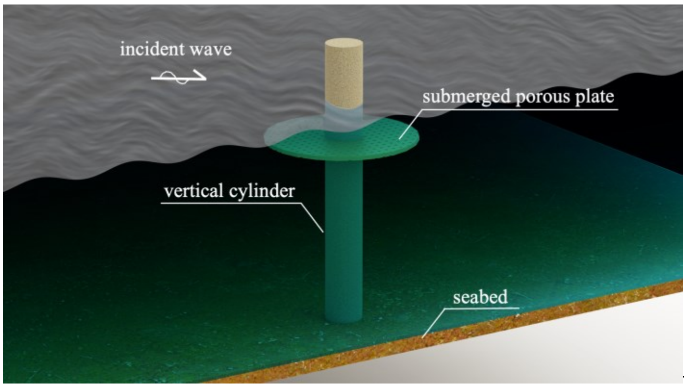

b)

Figure 1 a) Sketch and fluid domain division and b) 3-D diagram for a vertical cylinder with a submerged porous plate.

Under the framework of potential flow theory, the fluid can be described in terms of a time-dependent velocity potential $\Phi(r, \theta, z, t) = \mathrm{Re}[\phi(r, \theta, z)\mathrm{e}^{-\mathrm{i}\omega t}]$, where the symbol of Re[ ], i, and $\phi(r, \theta, z)$ represents real part of a complex, the imaginary unit, and the spatial velocity potential, respectively..

As shown in Fig. 1, the whole fluid domain is divided into three sub-regions, i.e., the outer region Ω_1 ($-d \le z \le 0$, $r \ge a$), the upper region above the plate Ω_2 ($-h_1 \le z \le 0$, $b \le r \le a$), and the region beneath the plate Ω_3 ($-d \le z \le -h_2$, $b \le r \le a$). The velocity potential in each sub-region Ω_j is denoted by ϕ_j (j = 1, 2 and 3), which satisfies the Laplace equation in corresponding sub-regions, i.e.,

$$\nabla^2 \phi_j = 0 . \tag{1}$$

The velocity potential also satisfies the appropriate boundary conditions on the free-surface and seabed, namely,

$$\frac{\partial \phi_j}{\partial z} = \frac{\omega^2}{g}\phi_j \text{ for } z = 0,\ j = 1 \text{ and } 2, \tag{2}$$

and

$$\frac{\partial \phi_j}{\partial z} = 0 \text{ for } z = -d,\ j = 1 \text{ and } 3, \tag{3}$$

where g is the gravitational acceleration. The boundary condition on the impermeable surface of the vertical cylinder can be expressed as

$$\frac{\partial \phi_2}{\partial r} = 0 \text{ for } r = b,\ -h_1 < z < 0, \tag{4}$$

and

$$\frac{\partial \phi_3}{\partial r} = 0 \text{ for } r = b,\ -d < z < -h_1. \tag{5}$$

Following Sollitt and Cross (1972) and Yu (1995), the boundary condition on the thin porous plate can be expressed as

$$\frac{\partial \phi_2}{\partial z} = \mathrm{i}k_0 G(\phi_3 - \phi_2) \text{ for } b < r < a,\ z = -h_1. \tag{6}$$

Here k_0 is the incident wavenumber, which is the positive real solution of the dispersion relation of $\omega^2 = gk_0\tanh(k_0 d)$; the complex porous coefficient of the submerged porous plate $G = \frac{\gamma}{k_0\delta}\left\{f - \mathrm{i}\left[1 + \frac{C_m(1-\gamma)}{\gamma}\right]\right\}^{-1}$; δ is the physical thickness of the porous plate; γ, f and C_m are the porosity, the linearized resistance coefficient, and the added-mass coefficient of the porous medium, respectively (Yu, 1995); G can be written as G_r + iG_i, where G_r denotes the real part and G_i the imaginary part. Physically, G_r and G_i represent the drag and the inertia effect of the porous plate, which lead to wave energy loss and phase change, respectively.

At the far field (i.e., $r \rightarrow \infty$), the velocity potential of ϕ_1 satisfies the condition of

$$\lim_{r\to\infty}\left[\sqrt{r}\left(\frac{\partial}{\partial r} - \mathrm{i}k_0\right)\left(\phi_1 - \phi_{\mathrm{I}}\right)\right] = 0, \tag{7}$$

where ϕ_{I} is the velocity potential of incident waves (i.e., $\phi_{\mathrm{I}} = \frac{-\mathrm{i}gA}{\omega}\sum_{m=0}^{\infty}\varepsilon_m \mathrm{i}^m \cos\left(m\theta\right)\mathrm{J}_m(k_0 r)Z_0(k_0 z)$). $\mathrm{J}_m(k_0 r)$ denotes the first kind of Bessel function of order m. $Z_0(k_0 z)$ represents the vertical eigenfunction, which is mathematically defined in Eq. (18).

On the interface between different sub-regions, the velocity potentials satisfy the following matching conditions:

$$\begin{cases} \dfrac{\partial \phi_1}{\partial r} = \dfrac{\partial \phi_2}{\partial r} & \text{for } -h_1 < z < 0,\ r = a \\ \dfrac{\partial \phi_1}{\partial r} = \dfrac{\partial \phi_3}{\partial r} & \text{for } -d < z < -h_1,\ r = a \\ \dfrac{\partial \phi_2}{\partial z} = \dfrac{\partial \phi_3}{\partial z} & \text{for } b < r < a,\ z = -h_1 \end{cases}, \tag{8}$$

and

$$\begin{cases} \phi_1 = \phi_2 & \text{for } -h_1 < z < 0, r = a \\ \dfrac{\partial \phi_2}{\partial z} = \mathrm{i}k_0 G\left(\phi_3 - \phi_2\right) & \text{for } b < r < a,\ z = -h_1 \\ \phi_1 = \phi_3 & \text{for } -d < z < -h_1, r = a \end{cases}. \tag{9}$$

The velocity potential of $\varphi_j (j = 2 \text{ and } 3)$ are linearly decomposed into two parts, namely

$$\phi_j = \phi_{j,v} + \phi_{j,h}. \tag{10}$$

For the present problem, the velocity potential of ϕ_j is linearly decomposed as $\phi_{j,v}$ and $\phi_{j,h}$. Hence, the velocity potential of $\phi_{j,v}$ and $\phi_{j,h}$ satisfy the Laplace equations. The velocity potentials of $\phi_{2,v}$, $\phi_{2,h}$, $\phi_{3,v}$, and $\phi_{3,h}$ satisfy the following boundary conditions:

$$\begin{cases} \dfrac{\partial \phi_{2,v}}{\partial z} = \dfrac{\omega^2}{g}\phi_{2,v} & \text{for } b < r < a,\ z = 0 \\ \dfrac{\partial \phi_{2,h}}{\partial z} = \dfrac{\omega^2}{g}\phi_{2,h} & \text{for } b < r < a,\ z = 0 \\ \dfrac{\partial \phi_{2,v}}{\partial z} = 0 & \text{for } b < r < a,\ z = -h_1 \\ \phi_{2,h} = 0 & \text{for } r = a \text{ or } b, -h_1 < z < 0 \end{cases}, \tag{11}$$

and

$$\begin{cases} \dfrac{\partial \phi_{3,v}}{\partial z} = 0 & \text{for } b < r < a,\ z = -d \\ \dfrac{\partial \phi_{3,h}}{\partial z} = 0 & \text{for } b < r < a,\ z = -d \\ \dfrac{\partial \phi_{3,v}}{\partial z} = 0 & \text{for } b < r < a,\ z = -h_1 \\ \phi_{3,h} = 0 & \text{for } r = a \text{ or } b, -d < z < -h_1 \end{cases}. \tag{12}$$

We note that the fluid domain of Ω_2 and Ω_3 is a ring region, which is different to the circular region as dispicted in Liu et al. (2011). This directly leads to the different form of corresponding boundary conditions (see Eqs. (12) and (13)). The velocity and pressure continuity conditions (i.e., Eqs. (8) and (9)) can be re-written as:

$$\begin{cases} \dfrac{\partial \phi_1}{\partial r} = \dfrac{\partial\left(\phi_{2,v}+\phi_{2,h}\right)}{\partial r} & \text{for } -h_1 < z < 0,\ r = a \\ \dfrac{\partial \phi_1}{\partial r} = \dfrac{\partial\left(\phi_{3,v}+\phi_{3,h}\right)}{\partial r} & \text{for } -d < z < -h_1,\ r = a \\ \dfrac{\partial \phi_{2,h}}{\partial z} = \dfrac{\partial \phi_{3,h}}{\partial z} & \text{for } b < r < a,\ z = -h_1 \\ \dfrac{\partial\left(\phi_{2,v}+\phi_{2,h}\right)}{\partial r} = 0 & \text{for } -h_1 < z < 0,\ r = b \\ \dfrac{\partial\left(\phi_{3,v}+\phi_{3,h}\right)}{\partial r} = 0 & \text{for } -d < z < -h_1,\ r = b \end{cases}, \tag{13}$$

and

$$\begin{cases} \phi_1 = \phi_{2,v} & \text{for } -h_1 < z < 0,\ r = a \\ \dfrac{\partial \phi_{2,h}}{\partial z} = \mathrm{i}k_0 G\left(\phi_{3,v}+\phi_{3,h}-\phi_{2,v}-\phi_{2,h}\right) & \text{for } b < r < a,\ z = -h_1 \\ \phi_1 = \phi_{3,v} & \text{for } -d < z < -h_1,\ r = a \end{cases}. \tag{14}$$

2.2 Analytical derivation

In this section, a semi-analytical solution of the wave diffraction problem defined in Section 2.1 is derived. In sub-region Ω_1, the velocity potential ϕ_1 can be written as

$$\phi_1 = \frac{-\mathrm{i}gA}{\omega}\sum_{m=0}^{\infty}\varepsilon_m \mathrm{i}^m \cos\left(m\theta\right)\left[\mathrm{J}_m(k_0 r)Z_0(k_0 z) + \sum_{l=0}^{\infty} A_{ml}^{(1)} U_m(k_l r) Z_l(k_l z)\right], \tag{15}$$

where $\varepsilon_0 = 1$ and $\varepsilon_m = 2$ ($m \geq 1$), A_{ml} (m, l = 0, 1, 2…) are unknown coefficients. The coefficients of k_l (l = 1, 2, 3 …) are the positive real solutions of the following dispersion relation,

$$\omega^2 = -gk_l \tan\left(k_l d\right). \tag{16}$$

The radial eigenfunctions $U_m(k_l r)$ are written as:

$$U_m(k_l r) = \begin{cases} \mathrm{H}_m^{(1)}(k_l r) & l = 0 \\ \mathrm{K}_m(k_l r) & l \geq 1 \end{cases}, \tag{17}$$

where $\mathrm{H}_m^{(1)}(k_l r)$ denotes the first kind of Hankel function of order m, $\mathrm{K}_m(k_l r)$ is the second kind of modified Bessel function of order m. The vertical eigenfunctions $Z_l(k_l z)$, which satisfy the orthogonal relation with respect of [-d, 0], can be written as

$$Z_l(k_l z)=\begin{cases}\cosh\left[k_l(z+d)\right]/\cosh\left(k_l d\right) & \text{for } l=0\\ \cos\left[k_l(z+d)\right]/\cos\left(k_l d\right) & \text{for } l\geq 1\end{cases}. \tag{18}$$

The scattered velocity potentials $\phi_{2,v}$ and $\phi_{2,h}$ in sub-region Ω_2, which satisfy free-surface and rigid body boundary conditions (i.e., Eqs. (2) and (4)), can be written as:

$$\phi_{2,v}=\frac{-\mathrm{i}gA}{\omega}\sum_{m=0}^{\infty}\varepsilon_m \mathrm{i}^m\cos\left(m\theta\right)\sum_{l=0}^{\infty}\left[A_{ml}^{(2)}P_m\left(\lambda_l r\right)+C_{ml}^{(1)}Q_m\left(\lambda_l r\right)\right]Y_l(\lambda_l z), \tag{19}$$

and

$$\phi_{2,h}=\frac{-\mathrm{i}gA}{\omega}\sum_{m=0}^{\infty}\varepsilon_m \mathrm{i}^m\cos\left(m\theta\right)\sum_{l=0}^{\infty}A_{ml}^{(3)}\left[\mathrm{J}_m(\beta_{ml}r)+D_{ml}^{(1)}\mathrm{Y}_m(\beta_{ml}r)\right]Q_{ml}\left(z\right), \tag{20}$$

where λ_l can be derived by the following relations

$$\omega^2=\begin{cases}g\lambda_l\tanh\left(\lambda_l h\right) & \text{for } l=0\\ -g\lambda_l\tan\left(\lambda_l h\right) & \text{for } l\geq 1\end{cases}. \tag{21}$$

By referring to Eqs. (11) and (13), the unknown coefficient of β_{ml} can be determined by substituting $\phi_{2,h}$ into corresponding boundary conditions, i.e., $\phi_{2,h}=0$ for $r=a$, $-h_1<z<0$, and $\partial\phi_{2,h}/\partial r=0$ for $r=b$, $-h_1<z<0$. Hence, we have

$$\beta_{ml}\mathrm{J}_{m-1}\left(\beta_{ml}b\right)\text{-}\mathrm{J}_m\left(\beta_{ml}b\right)/b-\frac{\mathrm{J}_m(\beta_{ml}a)}{\mathrm{Y}_m(\beta_{ml}a)}\left[\beta_{ml}\mathrm{Y}_{m-1}\left(\beta_{ml}b\right)\text{-}\mathrm{Y}_m\left(\beta_{ml}b\right)/b\right]=0. \tag{22}$$

We truncate the infinite series of β_{ml} as finite series by introducing the truncation number $\widehat{L}$ and $\widehat{M}$ (i.e., $l=0, 1,\ldots\widehat{L}$; $m=0, 1,\ldots\widehat{M}$). The implementation of truncation number $\widehat{L}$ and $\widehat{M}$ results in $\left[\left(\widehat{M}+1\right)\times\left(\widehat{L}+1\right)\right]$ unkowns to be solved.

The radial eigenfunctions $P_m(\lambda_l r)$ and $Q_m(\lambda_l r)$ in Eq. (19) are given by

$$P_m\left(\lambda_l r\right)=\begin{cases}\mathrm{J}_m(\lambda_l r) & \text{for } l=0\\ \mathrm{I}_m(\lambda_l r)/\mathrm{I}_m(\lambda_l a) & \text{for } l\geq 1\end{cases}, \tag{23}$$

and

$$Q_m\left(\lambda_l r\right)=\begin{cases}\mathrm{Y}_m(\lambda_l r) & \text{for } l=0\\ \mathrm{K}_m(\lambda_l r)/\mathrm{K}_m(\lambda_l a) & \text{for } l\geq 1\end{cases}, \tag{24}$$

respectively, where $\mathrm{I}_m(\,)$ denotes the first kind of modified Bessel function of order m, $\mathrm{K}_m(\,)$ denotes the second kind of modified Bessel function of order m. The vertical eigenfunctions $Y_l(\lambda_l z)$, which satisfy the orthogonal relation with respect of $[-h, 0]$, can be written as

$$Y_l(\lambda_l z)=\begin{cases}\cosh\left[\lambda_l(z+h_1)\right]/\cosh\left(\lambda_l h_1\right) & \text{for } l=0\\ \cos\left[\lambda_l(z+h_1)\right]/\cos\left(\lambda_l h_1\right) & \text{for } l\geq 1\end{cases}, \tag{25}$$

and $Q_{ml}(z)$ is written as

$$Q_{ml}\left(z\right)=\frac{\cosh\left(\beta_{ml}z\right)+\omega^2\sinh\left(\beta_{ml}z\right)/\left(g\beta_{ml}\right)}{\left[\omega^2/g-\beta_{ml}\tanh\left(\beta_{ml}h_1\right)\right]\cosh\left(\beta_{ml}h_1\right)}. \tag{26}$$

The velocity potentials $\phi_{3,v}$ and $\phi_{3,h}$ in Ω_3, which satisfy the seabed impermeable condtion and the boundary conditions shown in Eqs. (3) and (5), are given as:

$$\phi_{3,v}=\frac{-\mathrm{i}gA}{\omega}\sum_{m=0}^{\infty}\varepsilon_m\mathrm{i}^m\cos\left(m\theta\right)\sum_{l=0}^{\infty}\left[A_{ml}^{(4)}R_m(\kappa_l r)+C_{ml}^{(2)}S_m(\kappa_l r)\right]V_l(\kappa_l z), \tag{27}$$

and

$$\phi_{3,h}=\frac{-\mathrm{i}gA}{\omega}\sum_{m=0}^{\infty}\varepsilon_m\mathrm{i}^m\cos\left(m\theta\right)\sum_{l=0}^{\infty}A_{ml}^{(5)}\left[\mathrm{J}_m(\beta_{ml}r)+D_{ml}^{(2)}\mathrm{Y}_m(\beta_{ml}r)\right]T_{ml}\left(z\right), \tag{28}$$

where $\kappa_l=\mathrm{i}\pi/(d-h_1)$; the radial eigenfunctions $R_m(\kappa_l r)$ and $S_m(\kappa_l r)$ are defined as

$$R_m(\kappa_l r)=\begin{cases}1 & \text{for } m=0, l=0\\ \left(r/a\right)^m & \text{for } m\geq 1, l=0\\ \mathrm{I}_m(\kappa_l r)/\mathrm{I}_m(\kappa_l a) & \text{for } m\geq 0, l\geq 1\end{cases}, \tag{29}$$

and

$$S_m(\kappa_l r)=\begin{cases}\ln\left(r/a\right) & \text{for } m=0, l=0\\ \left(r/a\right)^{-m} & \text{for } m\geq 1, l=0\\ \mathrm{I}_m(\kappa_l r)/\mathrm{I}_m(\kappa_l a) & \text{for } m\geq 0, l\geq 1\end{cases}. \tag{30}$$

The vertical eigenfunctions $V_l(\kappa_l z)$, which satisfy the orthogonal relation with respect of $[-d, -h_1]$, can be written as

$$V_l(\kappa_l z)=\begin{cases}\sqrt{2}/2 & \text{for } l=0\\ \cos\left[\kappa_l(z+d)\right] & \text{for } l\geq 1\end{cases}, \tag{31}$$

and $T_{ml}(z)$ are given by

$$T_{ml}\left(z\right)=\frac{\cosh\left[\beta_{ml}\left(z+d\right)\right]}{\beta_{ml}\tanh\left(\beta_{ml}h_2\right)\cosh\left(\beta_{ml}h_2\right)}. \tag{32}$$

Inserting Eqs. (15), (19), (20), (27) and (28) into Eqs. (13) and (14), and then implementing the orthogonal relationship of the vertical, radial, and circular eigenfunctions, we obtain the following set of equations:

$$\begin{cases} \int_{-d}^{0} \frac{\partial \phi_1}{\partial r} Z_l(k_l z) dz = \int_{-h_1}^{0} \frac{\partial(\phi_{2,v}+\phi_{2,h})}{\partial r} Z_l(k_l z) dz + \int_{-d}^{-h_1} \frac{\partial(\phi_{3,v}+\phi_{3,h})}{\partial r} Z_l(k_l z) dz & \text{for } r=a \\ \int_b^a \frac{\partial \phi_{2,h}}{\partial z} \mathrm{J}_m(\beta_{ml} r) \mathrm{r} dr = \int_b^a \frac{\partial \phi_{3,h}}{\partial z} \mathrm{J}_m(\beta_{ml} r) \mathrm{r} dr & \text{for } z=-h_1 \\ \int_{-h_1}^{-0} \frac{\partial(\phi_{2,v}+\phi_{2,h})}{\partial r} Y_l(\lambda_l z) dz = 0 & \text{for } r=b \\ \int_{-d}^{-h_1} \frac{\partial(\phi_{3,v}+\phi_{3,h})}{\partial r} V_l(\kappa_l z) dz = 0 & \text{for } r=b \end{cases}, \quad (33)$$

and

$$\begin{cases} \int_{-h_1}^{0} \phi_1 Y_l(\lambda_l z) dz = \int_{-h_1}^{0} \phi_{2,v} Y_l(\lambda_l z) dz & \text{for } r=a \\ \int_{-d}^{-h_1} \phi_1 V_l(\kappa_l z) dz = \int_{-d}^{-h_1} \phi_{3,v} V_l(\kappa_l z) dz & \text{for } r=a \\ \int_{-d}^{0} \frac{\partial \phi_1}{\partial r} Z_l(k_l z) dz = \int_{-h_1}^{0} \frac{\partial(\phi_{2,v}+\phi_{2,h})}{\partial r} Z_l(k_l z) dz + \int_{-d}^{-h_1} \frac{\partial(\phi_{3,v}+\phi_{3,h})}{\partial r} Z_l(k_l z) dz & \text{for } r=a \end{cases}. \quad (34)$$

The above algebraic equations can be solved by standard matrix techniques. The unknown coefficients $A_{ml}^{(1)}$, $A_{ml}^{(2)}$, $A_{ml}^{(3)}$, $A_{ml}^{(4)}$, $A_{ml}^{(5)}$, $C_{ml}^{(1)}$, and $C_{ml}^{(2)}$ can be determined by truncating the infinite series in Eqs. (15), (19), (20), (27) and (28) to a finite term. Thus, the velocity potentials in relevant sub-regions can be determined. The corresponding details are shown in Appendix Eqs. (A1)~(A7).

The total horizontal force can be calculated by integrating the pressure on on surfaces $S_{b1}(-h_1 \le z \le 0, r = b)$ and $S_{b2}(-d \le z \le -h_1, r = b)$:

$$F_x = -\mathrm{i}\omega\rho \int_0^{2\pi} \int_{-h_1}^{0} \phi_2 \mathbf{n}_x r dz d\theta - \mathrm{i}\omega\rho \int_0^{2\pi} \int_{-d}^{-h_1} \phi_3 \mathbf{n}_x r dz d\theta, \quad (35)$$

where $\mathbf{n}_x = \cos\theta$, representing the normal vector in the x-direction. The force-induced bending moment regarding the point of (0, 0, $-d$) can be written as

$$M = -\mathrm{i}\omega\rho \begin{bmatrix} \int_0^{2\pi} \int_{-h_1}^{0} (\phi_{2,v}+\phi_{2,h}) \mathbf{n}_x rz dz d\theta + \int_0^{2\pi} \int_{-d}^{-h_1} (\phi_{3,v}+\phi_{3,h}) \mathbf{n}_x rz dz d\theta + \\ \int_0^{2\pi} \int_b^a (\phi_{3,v}+\phi_{3,h}-\phi_{2,v}-\phi_{2,h}) \mathbf{n}_z r^2 \cos\theta dr d\theta \end{bmatrix}, \quad (36)$$

where $\mathbf{n}_z$ represents the normal vector in the z-direction. Since $\int_0^{2\pi} \cos(m\theta)\cos\theta \mathrm{d}\theta = 0$ for $m = 0$ and $m \ge 2$, the total horizontal force F_x in Eq. (35) and the bending moment M in Eq. (36) can be calculated for $m = 1$. The vertical force F_z can be written as

$$F_z = -\mathrm{i}\omega\rho \int_0^{2\pi} \int_b^a (\phi_{3,v}+\phi_{3,h}-\phi_{2,v}-\phi_{2,h}) \mathbf{n}_z r dr d\theta \quad (37)$$

where $m = 0$ in ϕ_2 and ϕ_3, owing to $\int_0^{2\pi} \cos(m\theta) \mathrm{d}\theta = 0$ for $m \ge 1$.

The dimensionless wave amplitude can be calculated as

$$\frac{|\zeta|}{A}=\left|\frac{\mathrm{i}\omega}{gA}\phi_j\big|_{z=0}\right|,\ j=1 \text{ and } 2\,. \tag{38}$$

3. Numerical results and discussions

3.1 Validation

To examine the convergence of the semi-analytical solution, the horizontal force and wave amplitude at different truncated numbers $\hat{L}$ and $\widehat{M}$ are calculated in Table 1 and Table 2. The horizontal force $|F_x|$ and the wave amplitude $|\zeta|$ are nondimensionalized by ρgAb^2 and A, symbolically, $|F_x|/\rho gAb^2$ and $|\zeta|/A$, respectively.

Results of $|F_x|/\rho gAb^2$ for the different truncated number $\hat{L}$ is shown in Table 1. The geometrical wave parameters are fixed as b/d = 0.25, a/d = 0.5, h_1/d = 0.1, and G = 0.5 + 0.5i. From the results shown in Table 1, it is found that excellent convergence can be achieved as $\hat{L}$ = 20. Hence, the truncation number $\hat{L}$ of 20 was adopted throughout the calculations. Results of $|\zeta|/A$ with the different truncated number $\widehat{M}$ is shown in Table 2 (k_0d = 2). From the data presented in Table 2, we found that the semi-analytical solution converges at $\widehat{M}$ = 20.

Hence, in this paper, the calculations are conducted by setting the truncated number as $\hat{L}$ = 20 and $\widehat{M}$ = 20.

Table 1. Results of nondimensionalized horizontal force $|F_x|/\rho gAb^2$ with the different truncated numbers $\hat{L}$. The geometrical parameters are fixed as b/d = 0.25, a/d = 0.5, h_1/d = 0.1, and G = 0.5 + 0.5i.

Truncated number $\hat{L}$ ($\widehat{M}$ = 20)	Nondimensionalized horizontal force $|F_x|/\rho gAb^2$						
	k_0d = 0.5	k_0d = 1	k_0d = 2	k_0d = 3	k_0d = 5	k_0d = 7	k_0d = 10
3	2.944	4.984	6.142	6.611	6.057	4.717	3.474
5	2.944	4.987	6.157	6.618	5.991	4.599	3.366
8	2.945	4.989	6.162	6.616	5.968	4.570	3.345
15	2.945	4.989	6.162	6.614	5.959	4.558	3.335
20	2.945	4.989	6.163	6.614	5.955	4.553	3.331
25	2.945	4.989	6.163	6.614	5.955	4.553	3.331

Table 2. Results of nondimensionalized wave surface $|\zeta|/A$ with the different truncated numbers $\widehat{M}$. The geometrical and wave parameters are fixed as b/d = 0.25, a/d = 0.5, h_1/d = 0.1, G = 0.5 + 0.5i, and k_0d = 2.

Truncated numbers $\widehat{M}$ ($\hat{L}$ = 20)	Nondimensionalized wave surface $\lvert\zeta\rvert/A$ (θ = 0)						
	r/d = 0.3	r/d = 0.4	r/d = 0.6	r/d = 1	r/d = 1.5	r/d = 3	r/d = 5
0	1.465	1.212	0.628	0.126	1.154	0.199	0.220
5	2.097	1.850	1.307	1.153	1.092	1.514	1.347
10	2.097	1.850	1.307	1.154	1.116	1.080	0.987
15	2.097	1.850	1.307	1.154	1.116	1.081	1.064
20	2.097	1.850	1.307	1.154	1.116	1.081	1.061
25	2.097	1.850	1.307	1.154	1.116	1.081	1.061

We validate the present semi-analytical model with the published results in Wu and Chwang (2002). Note that the solution of the complex dispersion relationship (see Eq. (18) in Ref. (Chwang and Wu, 1994)) is required for the analytical model adopted in Wu and Chwang (2002). Besides, the evanescent-mode terms are not involved in Wu and Chwang's (2002) model. We also compare our results with numerical results calculated using a boundary element method (BEM) model (Mackay et al., 2021). Good agreement shown in Fig. 2 verifies the present alternative semi-analytical model.

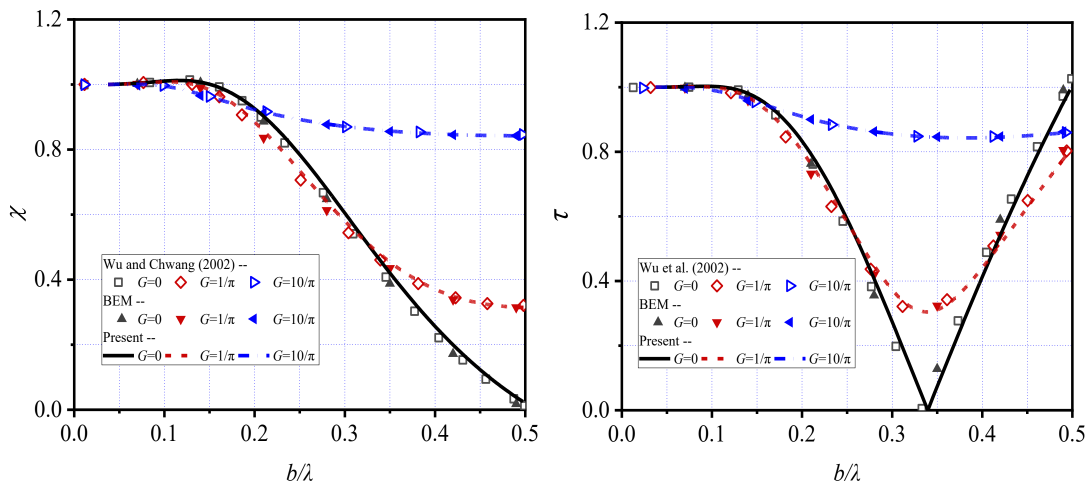

Figure 2 Comparisons of dimensionless horizontal force and bending moment obtained from the present model, Wu and Chwang (2002) and the numerical model (i.e., BEM). Geometrical/physical parameters are $h_1/d = 0.2$, $d/\lambda = 0.5$ and $b/a = 0.7$. λ indicates the incident wavelength satisfying the relation $\lambda = 2\pi/k$. χ and τ refer to F_b/F_∞ and M_b/M_∞, respectively. F_∞ and M_∞ denote the wave loads on a vertical cylinder without the porous plate.

3.2 Results and discussions

Following the above model validation, parametriccal studies were carried out to reveal the influence of the submerged plate on wave loads acting on the cylinder. In the paper, the moment center is taken at the bottom center of the vertical cylinder (0, 0, -d).

3.2.1 Effect of the porous coefficient

The effect of the porous coefficient is evaluated by considering $G = \varepsilon\,(1+1\mathrm{i})$, where $\varepsilon = 0$(i.e., 1E-7), 0.1, 0.5, 1, 2, 5, 20 and $+\infty$ (i.e., 1E7). Variation of $|F_x|/\rho g A b^2$, $|M|/\rho g A b^3$ and $|F_z|/\rho g A b^2$ against the dimensionless wave number $k_0 d$ for different porous coefficients are shown in Fig. 3.

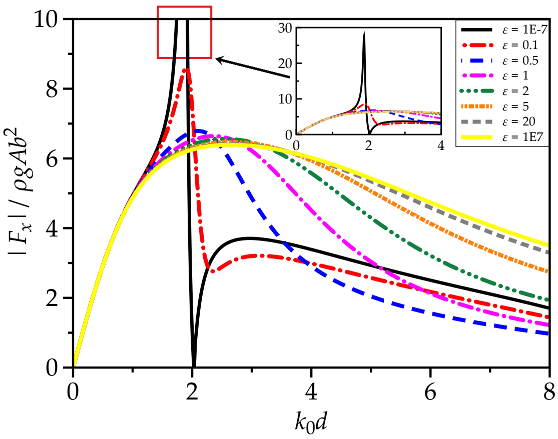

a)

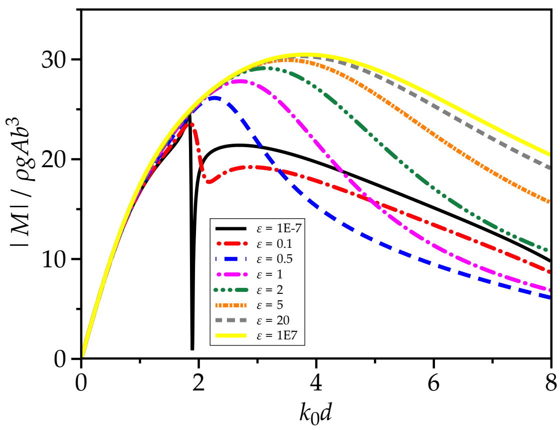

b)

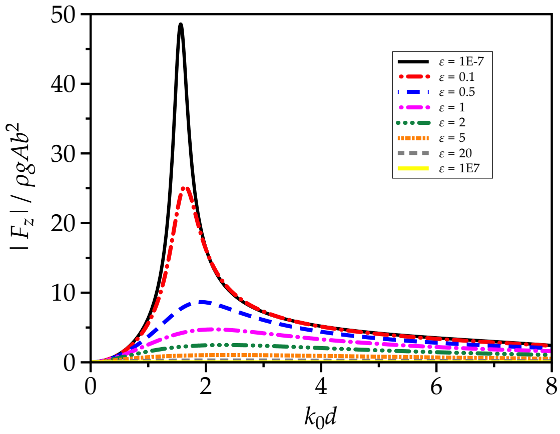

c)

Figure 3 Variation of $|F_x|/\rho g A b^2$, $|M|/\rho g A b^3$ and $|F_z|/\rho g A b^2$ for different porous coefficients. Geometrical parameters are fixed as $b/d = 0.15$, $a/d = 0.3$ and $h_1/d = 0.0125$.

From Fig. 3 (a~c), we observe that the horizontal/vertical force and force-induced bending moment are considerably mitigated by implementing the submerged porous plate for a certain frequency range. We also find a critical wavenumber k_c, beyond which the horizontal/vertical force and force-induced moment on the structure are reduced significantly. The wave force/moment approaches zeros at the critical wave number k_c. In contrast, for $k < k_c$, the horizontal and vertical wave loads experience a spike value as $G\to0$.

To clarify the physical meaning of the zero-value wave horizontal wave force, we plot the results of horizontal wave force (F_x), added mass (μ) and radiation damping (υ) in the sway mode of the vertical cylinder in Fig. 4, which are calculated by solving the corresponding sway-mode radiation problem (Li et al., 2022). Comparing the results in Fig. 3 a) and Fig. 4, we observe that zero-value horizontal force on the cylinder in the scattering problem corresponding to null radiation damping and the rapid changes of the added mass in sway mode. That is to say, there are no radiated waves in sway mode if the cylinder experiences forced motion with the critical frequency (i.e., corresponding to k_c).

Besides, we solved the heave-mode radiation problem of the present structure. The related velocity and pressure continuity conditions are given in Appendix Eqs. (A8)~(A9). Fig. 5 shows the results of vertical wave force (F_z), added mass (μ) and radiation damping (υ) in heave mode. From Fig. 5, we observe that location of the peak vertical force corresponds to that of the peak radiation damping and the rapid changes of the added mass. Previously, Martin and Farina (1997) and Zhao et al. (2017) also found those features theoretically. However, they did not thoroughly explain the relevance between the radiation problem and the diffraction problem at the critical frequency.

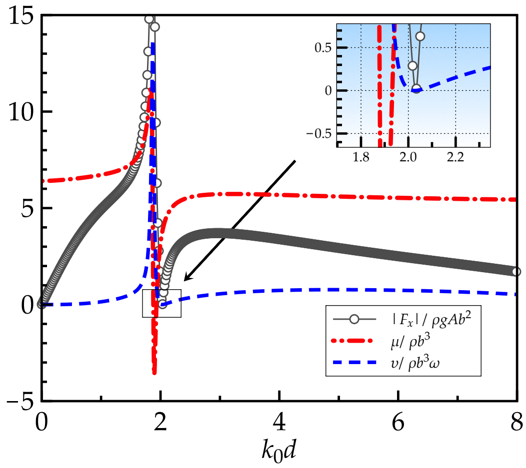

Figure 4. Variations of the horizontal wave exciting force, added mass and radiation damping. Geometrical/physical parameters fixed $G = 0$, $b/d = 0.15$, $a/d = 0.3$ and $h_1/d = 0.0125$.

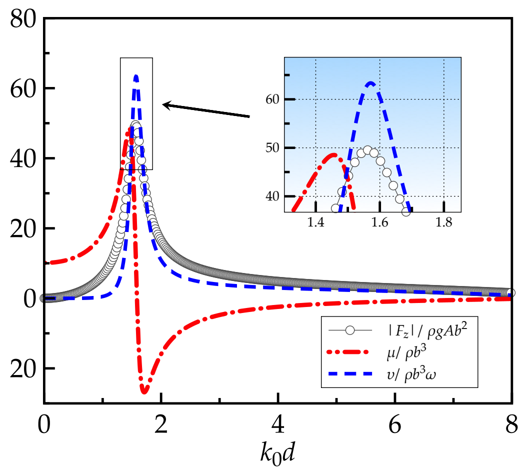

Figure 5. Variations of the vertical exciting force, added mass and radiation damping. Geometrical/physical parameters are fixed as $G = 0$, $b/d = 0.15$, $a/d = 0.3$ and $h_1/d = 0.0125$.

As the porous coefficient G increases, the submerged porous plate becomes a 'transparent' plate. The horizontal force/moment are modified significantly and approaches to that corresponding to the 'pure' cylinder at $k > k_c$. However, for $k < k_c$, G affects the moment slightly. In general, the frequency range of $k > k_c$ may be of significance from the point of view of wave loads mitigation. It is essential to note that properly setting the porous coefficient is key for reducing wave loads. As for present calculations, G of 0.5+0.5i may maximize the reduction of wave loads.

In general, G affects the wave loads significantly. For cases of ε approaches 0, the wave amplification above the plate lead to the soaring of the vertical wave force at $k = k_c$. However, the energy dissipation caused by the porosity leads to the wave loads reduction at $k > k_c$ for cases of ε = 0.5~2.

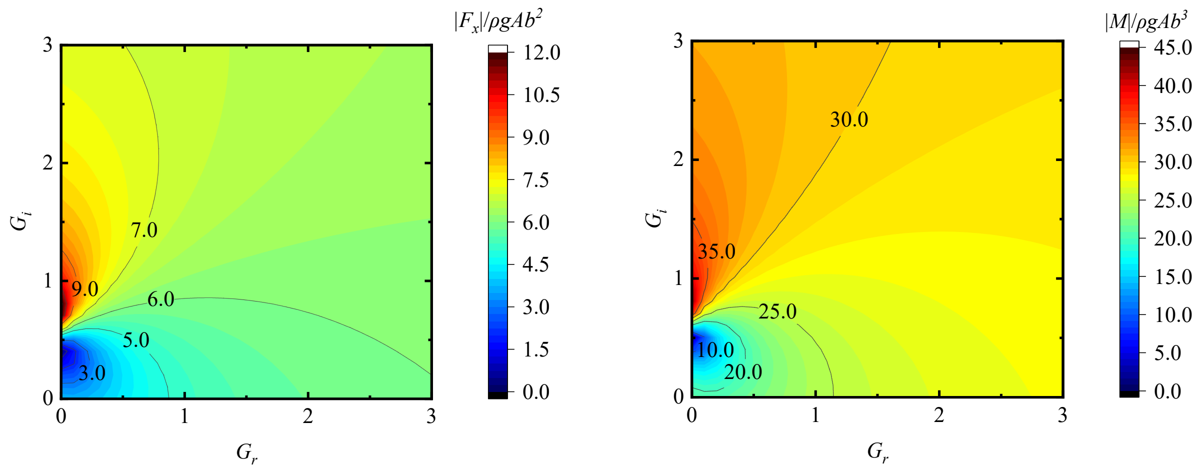

a) b)

Figure 6. Variations of $|F_x|/\rho gAb^2$ and $|M|/\rho gAb^3$. Geometrical/wave parameters are fixed $k_0d = 3$, $b/d = 0.15$, $a/d = 0.3$, $h_1/d = 0.0125$.

Here we investigate the influence of G_i and G_r on wave loads on the structure for the case of k_0d = 3. From Fig. 6, the minimum of wave loads is observed at (0, 0.5) approximately. And the minimum of wave loads cannot be found at the horizontal axis. This is due to the fact that the inertial and drag components of G affect the loads via different mechanisms. G_i modifies the wave loads by changing the phase difference of wave motion. However, G_r denotes the energy loss and dominates the load mitigation caused by the porous plate.

Fig. 7 (a-d) shows the wave amplitude distributions surrounding the vertical cylinder for different porous coefficient (i.e., $G = \varepsilon\cdot(1+1\mathrm{i})$, ε= 1E-7, 0.5, 2, 1E7). It is observed that the porous plate can positively suppress the wave run-up of the cylinder. Compared with a pure cylinder, the wave setdown occurs at the rear edge of the cylinder with a solid plate. Within the scope of the present calculations, the wave run-up on the cylinder is mitigated maximally for G = 0.5(1+1i).

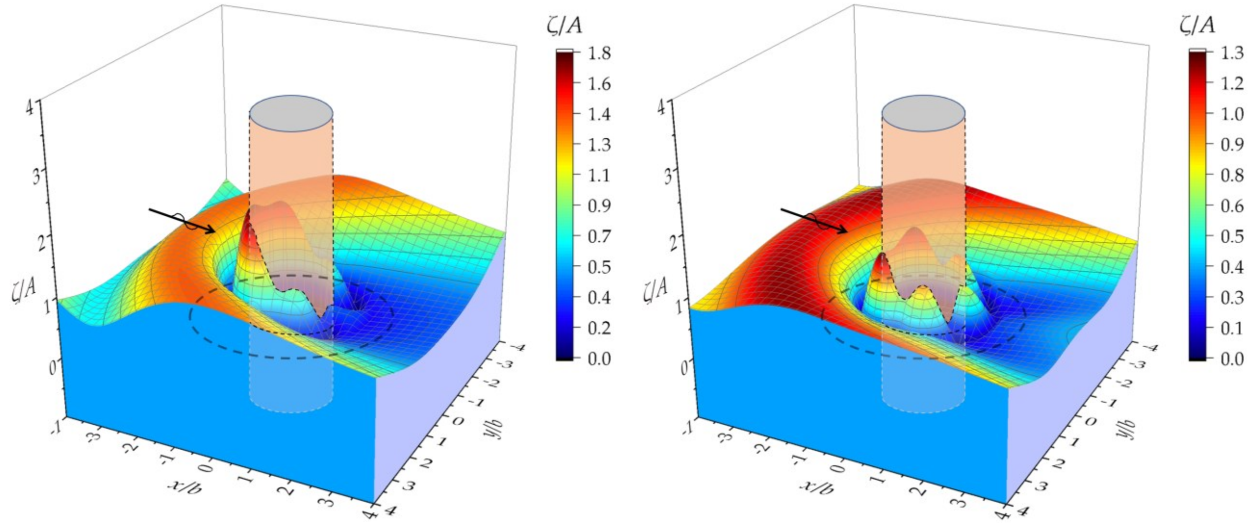

a) G = 0(i.e. 1E-7·(1+1i))

b) G = 0.5·(1+1i)

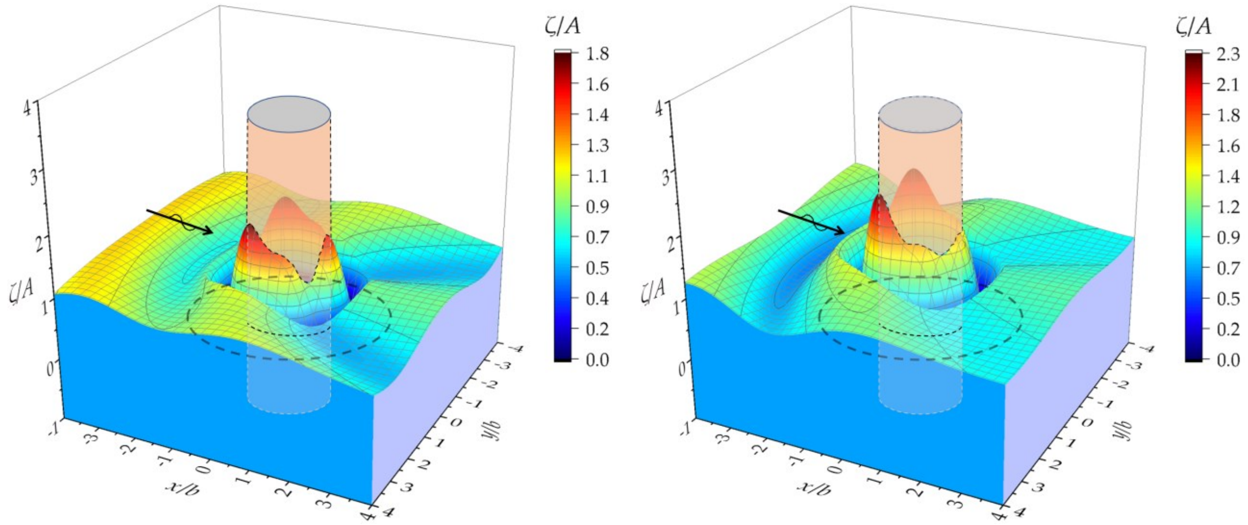

c) $G = 2\cdot(1+1i)$ d) $G = +\infty$(i.e. 1E7·(1+1i))

Figure 7 Three-dimensional wave amplitude distributions at a) $G = 0$(i.e. 1E-7·(1+1i)), b) $G = 0.5\cdot(1+1i)$, c) $G = 2\cdot(1+1i)$ and d) $G = +\infty$(i.e. 1E7·(1+1i)). Geometrical/physical parameters are fixed as $k_0d = 6$, $b/d = 0.15$, $a/d = 0.3$, $h_1/d = 0.0125$.

3.2.2 Effect of the submergence

The influence of the submergence of the porous plate on the hydrodynamic forces (F_x, M) is of interest from point of view of structure design. The parameters are fixed as $b/d = 0.15$, $a/d = 0.3$ and $G = 0.5(1+1i)$. Numerical calculations were performed with different draft of $h_1/d = 0.0125$, 0.025, 0.05, 0.1, 0.25, 0.5, 0.75 and 0.95. The variations of $|F_x|/\rho gAb^2$, and $|M|/\rho gAb^3$ as a function of the dimensionless wavenumber k_0d for different plate draft is shown in Fig. 8.

From the results shown in Fig. 8, it can be observed that the submergence affects the wave loads on the cylinder significantly. The remarkable load reduction is found for smaller draft. However, the load reduction becomes milder as the submergence increases. Moreover, the location of peak load shifts to high frequency range as the draft increases.

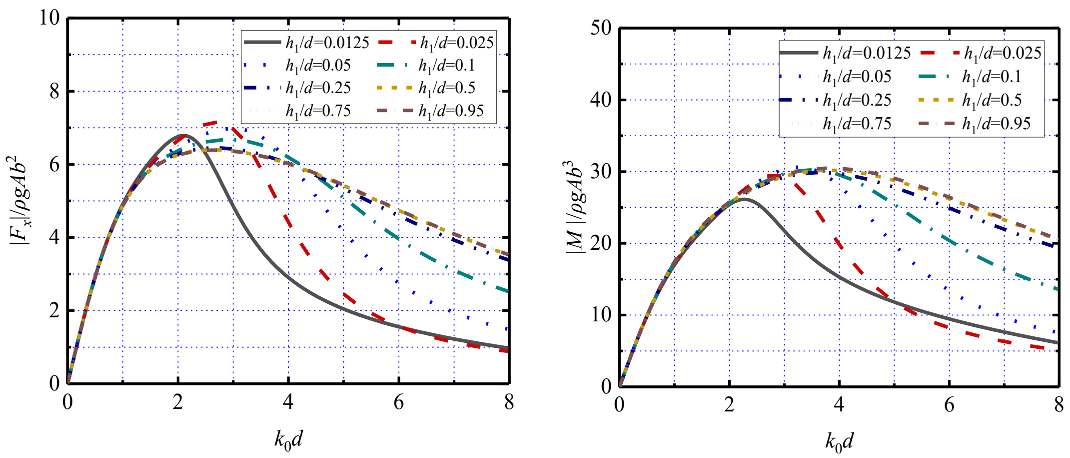

a) b)

Figure 8 Variation of $|F_x|/\rho gAb^2$ and $|M|/\rho gAb^3$ for different drafts of the porous plate, h_1. Geometrical/physical parameters are $b/d = 0.15$, $a/d = 0.3$, and $G = 0.5(1+1i)$.

3.2.3 Effect of the radius of a submerged porous plate

In this section, we explore the impact of the plate radius on the hydrodynamic characteristics of the cylinder. The effect of the submerged plate radius is evaluated by varying a/b as 1.375, 1.5, 1.625, and 1.75. The variation of $|F_x|/\rho gAb^2$ and $|M|/\rho gAb^3$ against the dimensionless wavenumber k_0d for different plate radius are shown in Fig. 9.

From Fig. 9 (a-b), we observe that the plate radius significantly affect the horizontal force and force-induced bending moment. As the plate radius increases, the horizontal force and force-induced bending moment have an similar trend. It is worth noting that the location of the minimum horizontal force/moment shifts to higher frequency range as the plate radius decrease.

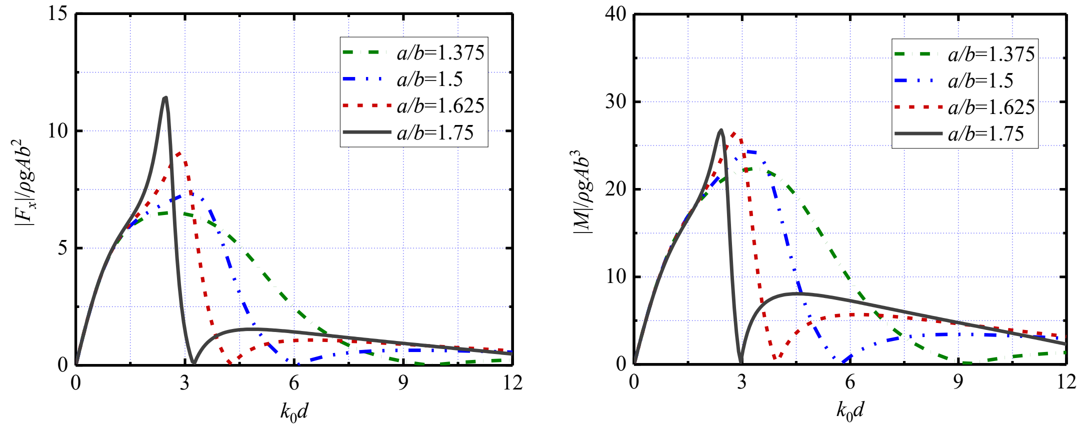

a) b)

Figure 9 Variation of $|F_x|/\rho gAb^2$ and $|M|/\rho gAb^3$ for different plate radiu. Geometrical/physical parameters are b/d = 0.2, h_1/d = 0.025.

3.2.4 Hydrodynamic characteristics of the cylinder in irregular waves

The analysis of the above results was carried out based on monochromatic waves, while the hydrodynamic characteristics of the cylinder in irregular waves are of interest in realistic cases. The velocity potential of the irregular waves can be obtained by summing the velocity potential of each wave component:

$$\Psi\left(x,z,t\right)=\mathrm{Re}\left[\sum_{n=1}^{N_f}\psi_n\left(x,z\right)e^{-\mathrm{i}\omega_n t}\right]. \quad (39)$$

In this section, we adapt the JONSWAP spectrum as the target spectrum, whose spectral density function can be written as

$$S(f)=\frac{\alpha g^2}{(2\pi)^4}\frac{1}{f^5}\exp\left[-\frac{5}{4}\left(\frac{f_p}{f}\right)^4\right]\gamma^{\exp\left[-\left(f-f_p\right)^2/\left(2\sigma^2 f_p^2\right)\right]}, \quad (40)$$

where α is the wave spectrum energy scale parameter, whose value is related to the significant wave height (H_s), $\alpha = 0.1$, f_p is wave spectrum peak frequency, γ is the peak enhancement factor, $\gamma = 3.3$, the value of peak shape coefficient σ is chosen as

$$\sigma = \begin{cases} \sigma_a = 0.07 & f < f_p \\ \sigma_b = 0.09 & f > f_p \end{cases}. \tag{41}$$

We separated the frequency range of $0.5f_p$ -$3.0f_p$ as N components and defined the wave amplitude of the ith component as a_i (i=1, …, N). Here, a particular form of irregular wave group (Tromans et al., 1991) is used to calculate assign the amplitude of the ith wave component:

we use the NewWave type irregular wave to calculate assign the amplitude of the ith wave component:

$$a_i = A_{\max} S\left(f_i\right)\Delta f_i \,/\, \sum_{i=1}^{N} S\left(f_i\right)\Delta f_i , \tag{42}$$

where $S(f_i)$ is the wave energy spectrum corresponds to the ith wave component, Δf_i is the frequency resolution ($\Delta f_i = 2.5f_p /N$) and $A_{\max}$ is the maximum amplitude which equals to the summation of a_i.

Considering that each wave component satisfies the Laplace equation and appropriate boundary conditions in the corresponding fluid region, the derivation of the corresponding velocity potential expression refers to section 2.2. The total horizontal force and moment can be calculated as

$$\begin{aligned} F_{\mathrm{x,irr}} &= F_{\mathrm{x1,irr}} + F_{\mathrm{x2,irr}} \\ &= \mathrm{i}\omega_f \rho \sum_{i=1}^{N} \left(\int_0^{2\pi}\int_{-h_1}^{0} \phi_2 \mathbf{n}_{\mathrm{x}} r \mathrm{d}z\mathrm{d}\theta + \int_0^{2\pi}\int_{-d}^{-h_1} \phi_3 \mathbf{n}_{\mathrm{x}} r \mathrm{d}z\mathrm{d}\theta \right), \end{aligned} \tag{43}$$

$$\begin{aligned} M_{\mathrm{irr}} &= M_{\mathrm{1,irr}} + M_{\mathrm{2,irr}} + M_{\mathrm{3,irr}} \\ &= -\mathrm{i}\omega_f \rho \sum_{i=1}^{N} \left(\begin{aligned} &\int_0^{2\pi}\int_{-h_1}^{0} \left(\phi_{2,v} + \phi_{2,h}\right) \mathbf{n}_{\mathrm{x}} rz \mathrm{d}z\mathrm{d}\theta + \int_0^{2\pi}\int_{-d}^{-h_1} \left(\phi_{3,v} + \phi_{3,h}\right) \mathbf{n}_{\mathrm{x}} rz \mathrm{d}z\mathrm{d}\theta + \\ &\int_0^{2\pi}\int_{b}^{a} \left(\phi_{3,v} + \phi_{3,h} - \phi_{2,v} - \phi_{2,h}\right) \mathbf{n}_{\mathrm{z}} rx \mathrm{d}r\mathrm{d}\theta \end{aligned} \right), \end{aligned} \tag{44}$$

where ω_f is the spectral density angular frequency.

Variations of $F_{\mathrm{x,irr}}/\rho g A b^2$ and $M_{\mathrm{irr}}/\rho g A b^3$ against $k_f d$ for different porous coefficients are shown in Fig. 10. The geometrical parameters are fixed as $b/d = 0.15$, $h_1/d = 0.025$ and $G = 0.5(1+1\mathrm{i})$. The effect of the porous coefficient is evaluated by considering $G = \varepsilon(1+1\mathrm{i})$, where $\varepsilon = 0$, 0.1, 0.5, 1, 2, 5, 20 and 1E7.

From Figs. 10 (a-b), it can be observed that the curves of the total horizontal wave force and overturning moment on the porous structure in irregular waves demonstrate similar trend as that in regular waves. Interestingly, null value of wave force/moment at the critical wave number was canceled due to the weighted average of the spectral density of the spectrum. In addition, the spike of the wave force/moment is also canceled.. Recalling Fig. 3, the frequency bandwidth corresponding to the null value of F_x and M is very narrow for $\varepsilon = 0$.

However, the critical frequency still exists for cases of irregular waves, beyond which the wave load mitigation can be observed. The wave loads/moment on a vertical cylinder with porous plate are smaller than those on a pure vertical cylinder in irregular waves at the interesting frequency region, which means the wave loads on the cylinder shall be positively suppressed by integrating with porous structure in irregular waves.

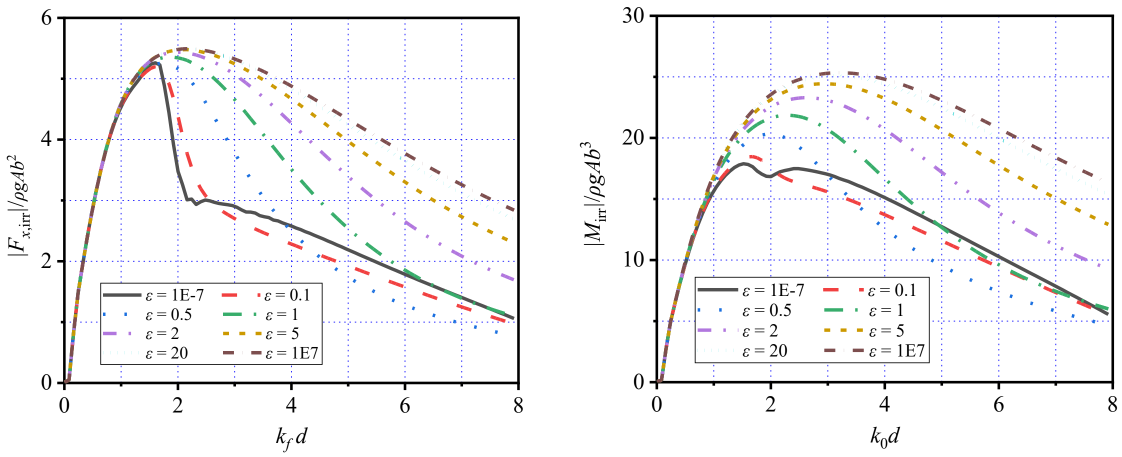

a) b)

Figure 10 Variation of $F_x/\rho gAb^2$ and $M/\rho gAb^3$ for different porous coefficients of G=(1+1i)·ε in irregular waves. Geometrical parameters are fixed as $b/d = 0.15$、$a/d = 0.3$ and $h_1/d = 0.125$

4. Concluding remarks

This paper considers an extension of earlier work (Wu and Chwang, 2002) and has developed an alternative semi-analytical solution for wave interaction on a vertical cylinder with a submerged porous plate. The model is validated by comparing with published analytical results and numerical results from a BEM solver. The solution of the complex dispersion relation (caused by the horizontal porous plate) is not required for the present method. In addition, compared with Wu and Chwang's (2002) solution, the evanescent mode waves are considered mathematically. In contrast to the solution for a submerged porous plate, additional auxiliary radial eigenfunctions in the ring region are needed.

Theoretical investigations have been carried out to explore the effect of various geometrical/ physical parameters. Wave loads are mitigated effectively in the presence of the submerged porous plate among a certain frequency region. A critical wavenumber k_c corresponds to the lower threshold of a loads mitigation region. For a solid plate, k_c corresponds to the presence of the null radiation damping and the obvious changes of added mass for the structure in sway mode.

Wave loads on the cylinder are mitigated remarkably for the frequency region of $k > k_c$ as the porous coefficient decreases. But, for $k < k_c$, the horizontal and vertical wave loads experience a spike value as $G \rightarrow 0$, which should be avoided in practical engineering.

It is expected that the results obtained in this work will provide the necessary background for designing appropriate and efficient structures for reducing wave loads on an offshore pile. Future investigations considering wave nonlinearity or extreme waves are of interest.

Acknowledgments

The authors would like to acknowledge the financial support of the Key Program for International Scientific and Technological Innovation Cooperation between Governments (2019YFE0102500), the National Natural Science Foundation of China (52001086), and the China Postdoctoral Science Foundation funded project (2019M661257). This work was part-funded under EPSRC ResIn project, United Kingdom grant EP/R007519/1.

Appendix

The expressions of diffraction potential in detail are shown as

$$\phi_1 = \frac{-\mathrm{i}gA}{\omega}\sum_{m=0}^{\infty}\varepsilon_m \mathrm{i}^m \cos(m\theta)\left\{\mathrm{J}_m(k_0 r)Z_0(k_0 z)+A_{m0}^{(1)}\mathrm{H}_m^{(1)}(k_0 r)Z_0(k_0 z)+\sum_{l=1}^{\infty}A_{ml}^{(1)}\mathrm{K}_m(k_l r)Z_l(k_l z)\right\}, \quad \text{(A1 a)}$$

$$\phi_{2,v} = \frac{-\mathrm{i}gA}{\omega}\sum_{m=0}^{\infty}\varepsilon_m \mathrm{i}^m \cos(m\theta)\left\{\left(A_{m0}^{(2)}\mathrm{J}_m(\lambda_0 r)+C_{m0}^{(1)}\mathrm{Y}_m(\lambda_0 r)\right)Y_0(\lambda_0 z)+\sum_{l=1}^{\infty}\left[A_{mi}^{(2)}\frac{\mathrm{I}_m(\lambda_l r)}{\mathrm{I}_m(\lambda_l a)}+C_{ml}^{(1)}\frac{\mathrm{K}_m(\lambda_l r)}{\mathrm{K}_m(\lambda_l a)}\right]Y_l(\lambda_l z)\right\}, \quad \text{(A1 b)}$$

$$\phi_{2,h} = \frac{-\mathrm{i}gA}{\omega}\sum_{m=0}^{\infty}\varepsilon_m \mathrm{i}^m \cos(m\theta)\left\{\sum_{m=0}^{\infty} A_{ml}^{(3)}\left[\mathrm{J}_m(\beta_{ml}r)+D_{ml}^{(1)}\mathrm{Y}_m(\beta_{ml}r)\right]\frac{\cosh\beta_{ml}z+\dfrac{\omega^2}{g\beta_{ml}}\sinh\beta_{ml}z}{\left(\dfrac{\omega^2}{g}-\beta_{ml}\tanh\beta_{ml}h_1\right)\cosh(\beta_{ml}h_1)}\right\}, \quad \text{(A1 c)}$$

$$\phi_{3,v} = \begin{cases} \dfrac{-\mathrm{i}gA}{\omega}\displaystyle\sum_{m=0}^{\infty}\varepsilon_m \mathrm{i}^m \cos(m\theta)\left\{\left[A_{m0}^{(4)}+C_{m0}^{(2)}\ln\left(\frac{r}{a}\right)\right]V_0(\kappa_0 z)+\sum_{l=1}^{\infty}\left[A_{ml}^{(4)}\frac{\mathrm{I}_m(\kappa_l r)}{\mathrm{I}_m(\kappa_l a)}+C_{ml}^{(2)}\frac{\mathrm{K}_m(\kappa_l r)}{\mathrm{K}_m(\kappa_l a)}\right]V_l(\kappa_l z)\right\}, & m=0 \\ \dfrac{-\mathrm{i}gA}{\omega}\displaystyle\sum_{m=0}^{\infty}\varepsilon_m \mathrm{i}^m \cos(m\theta)\left\{\left[A_{m0}^{(4)}\left(\frac{r}{a}\right)^m+C_{m0}^{(2)}\left(\frac{r}{a}\right)^{-m}\right]V_0(\kappa_0 z)+\sum_{l=1}^{\infty}\left[A_{ml}^{(4)}\frac{\mathrm{I}_m(\kappa_l r)}{\mathrm{I}_m(\kappa_l a)}+C_{ml}^{(2)}\frac{\mathrm{K}_m(\kappa_l r)}{\mathrm{K}_m(\kappa_l a)}\right]V_l(\kappa_l z)\right\}, & m\geq 1 \end{cases},$$

$$\text{(A1 d)}$$

and

$$\phi_{3,h} = \frac{-\mathrm{i}gA}{\omega}\sum_{m=0}^{\infty}\varepsilon_m \mathrm{i}^m \cos(m\theta)\left\{\sum_{m=0}^{\infty} A_{mi}^{(5)}\left[\mathrm{J}_m(\beta_{ml}r)+D_{ml}^{(2)}\mathrm{Y}_m(\beta_{ml}r)\right]\frac{\cosh\beta_{ml}(z+d)}{\beta_{ml}\tanh\beta_{ml}h_2\cosh\beta_{ml}h_2}\right\}, \quad \text{(A1 e)}$$

where $A_{m1}^{(1)}$, $A_{ml}^{(2)}$, $A_{ml}^{(3)}$, $A_{ml}^{(4)}$, $A_{ml}^{(5)}$, $C_{ml}^{(1)}$, and $C_{ml}^{(2)}$ are unknown coefficients of scatting potential.

Substituting the diffraction potentials (i.e., Eqs. (A1 a) ~ (A1 e) in Appendix) into the velocity and pressure continuity conditions (i.e., Eqs. (33) and (34)) at the interfaces between the adjacent subdomains, employing orthogonal relation, truncating the velocity potential expressions as a finite series (i.e., the upper bound of m and l are selected as $\widehat{M}$ and $\widehat{L}$, respectively), a set of linear equations corresponding to the scatting problem are expressed as

$$[\Xi]\cdot[X]=[\mathrm{B}], \quad \text{(A2)}$$

where the matrix of $[\Xi]$ can be expressed as

$$[\Xi]=\begin{bmatrix} [\Xi]_{ml\iota}^{1,1} & -[\Xi]_{ml\iota}^{1,2} & 0 & 0 & 0 & -[\Xi]_{ml\iota}^{1,6} & 0 \\ [\Xi]_{ml\iota}^{2,1} & 0 & 0 & -[\Xi]_{ml\iota}^{2,4} & 0 & 0 & -[\Xi]_{ml\iota}^{2,7} \\ [\Xi]_{ml\iota}^{3,1} & -[\Xi]_{ml\iota}^{3,2} & -[\Xi]_{ml\iota}^{3,3} & -[\Xi]_{ml\iota}^{3,4} & -[\Xi]_{ml\iota}^{3,5} & -[\Xi]_{ml\iota}^{3,6} & -[\Xi]_{ml\iota}^{3,7} \\ 0 & -[\Xi]_{ml\iota}^{4,2} & [\Xi]_{ml\iota}^{4,3} & -[\Xi]_{ml\iota}^{4,4} & -[\Xi]_{ml\iota}^{4,5} & -[\Xi]_{ml\iota}^{4,6} & -[\Xi]_{ml\iota}^{4,7} \\ 0 & 0 & [\Xi]_{ml\iota}^{5,3} & 0 & -[\Xi]_{ml\iota}^{5,5} & 0 & 0 \\ 0 & [\Xi]_{ml\iota}^{6,2} & [\Xi]_{ml\iota}^{6,3} & 0 & 0 & [\Xi]_{ml\iota}^{16,6,1} & 0 \\ 0 & 0 & 0 & [\Xi]_{ml\iota}^{7,4} & [\Xi]_{ml\iota}^{7,5} & 0 & [\Xi]_{ml\iota}^{7,7} \end{bmatrix}. \quad \text{(A3)}$$

The matrix of $[\mathrm{B}]$ can be expressed as

$$[\mathrm{B}]=\left[-\left\{e_{ml\iota}^{(1)}\right\} \quad -\left\{e_{ml\iota}^{(2)}\right\} \quad -\left\{e_{ml\iota}^{(3)}\right\} \quad 0 \quad 0 \quad 0\right]^T. \quad \text{(A4)}$$

The components $[\mathrm{B}]$ are as follows

$$e_{ml\iota}^{(1)} = \sum_{m=0}^{\hat{M}}\int_{-h_1}^{0}\mathrm{J}_m(k_0 a)Z_0(k_0 z)\sum_{\iota=0}^{\hat{L}}Y_\iota(\lambda_\iota z)\mathrm{d}z, \quad m\geq 0,\, l=0,\, \iota\geq 0, \quad \text{(A5 a)}$$

$$e_{ml\iota}^{(2)} = \sum_{m=0}^{\hat{M}} \int_{-d}^{-h_1} \mathrm{J}_m(k_0 a) Z_0(k_0 z) \sum_{\iota=0}^{\hat{L}} V_\iota(\kappa_\iota z) \mathrm{d}z, \quad m \ge 0, l = 0, \iota \ge 0, \tag{A5 b}$$

and

$$e_{ml\iota}^{(3)} = \sum_{m=0}^{\hat{M}} \int_{-d}^{0} k_0 \mathrm{J}_m{}'(k_0 a) Z_0(k_0 z) \sum_{\iota=0}^{\hat{L}} Z_\iota\left(k_\iota z\right) \mathrm{d}z, \quad m \ge 0, l = 0, \iota \ge 0. \tag{A5 c}$$

The matrix of $[X]$ which represent the unknown coefficients, is given by

$$[\mathrm{X}] = \left[A_{ml}^{(1)} \quad A_{ml}^{(2)} \quad A_{ml}^{(3)} \quad A_{ml}^{(4)} \quad A_{ml}^{(5)} \quad C_{ml}^{(1)} \quad C_{ml}^{(2)} \right]^T. \tag{A6}$$

The components of $[\Xi]$ are as follows:

$$[\Xi]_{ml\iota}^{1,1} = \begin{cases} \sum_{m=0}^{\hat{M}} \int_{-h_1}^{0} \mathrm{H}_m^{(1)}(k_0 a) Z_0(k_0 z) \sum_{\iota=0}^{\hat{L}} Y_\iota(\lambda_\iota z) \, \mathrm{d}z, & m \ge 0, l = 0, \iota \ge 0 \\ \sum_{m=0}^{\hat{M}} \int_{-h_1}^{0} \sum_{l=1}^{\hat{L}} \mathrm{K}_m(k_l a) Z_l(k_l z) \sum_{\iota=0}^{\hat{L}} Y_\iota(\lambda_\iota z) \, \mathrm{d}z, & m \ge 0, l \ge 1, \iota \ge 0 \end{cases}, \tag{A7 a}$$

$$[\Xi]_{ml\iota}^{1,2} = \begin{cases} \sum_{m=0}^{\hat{M}} \int_{-h_1}^{0} \mathrm{J}_m(\lambda_0 a) Y_0(\lambda_0 z) \sum_{\iota=0}^{\hat{L}} Y_\iota(\lambda_\iota z) \, \mathrm{d}z, & m \ge 0, l = 0, \iota \ge 0 \\ \sum_{m=0}^{\hat{M}} \int_{-h_1}^{0} \sum_{l=1}^{\hat{L}} Y_l(\lambda_l z) \sum_{\iota=0}^{\hat{L}} Y_\iota(\lambda_\iota z) \, \mathrm{d}z, & m \ge 0, l \ge 1, \iota \ge 0 \end{cases}, \tag{A7 b}$$

$$[\Xi]_{ml\iota}^{1,6} = \begin{cases} \sum_{m=0}^{\hat{M}} \int_{-h_1}^{0} \mathrm{Y}_m(\lambda_0 a) Y_0(\lambda_0 z) \sum_{\iota=0}^{\hat{L}} Y_\iota(\lambda_\iota z) \, \mathrm{d}z, & m \ge 0, l = 0, \iota \ge 0 \\ \sum_{m=0}^{\hat{M}} \int_{-h_1}^{0} \sum_{l=1}^{\hat{L}} Y_l(\lambda_l z) \sum_{\iota=0}^{\hat{L}} Y_\iota(\lambda_\iota z) \, \mathrm{d}z, & m \ge 0, l \ge 1, \iota \ge 0 \end{cases}, \tag{A7 c}$$

$$[\Xi]_{ml\iota}^{2,1} = \begin{cases} \sum_{m=0}^{\hat{M}} \int_{-d}^{-h_1} \mathrm{H}_m^{(1)}(k_0 a) Z_0(k_0 z) \sum_{\iota=0}^{\hat{L}} V_\iota(\kappa_\iota z) \, \mathrm{d}z, & m \ge 0, l = 0, \iota \ge 0 \\ \sum_{m=0}^{\hat{M}} \int_{-d}^{-h_1} \sum_{l=1}^{\hat{L}} \mathrm{K}_m(k_i a) Z_l(k_l z) \sum_{\iota=0}^{\hat{L}} V_\iota(\kappa_\iota z) \, \mathrm{d}z, & m \ge 0, l \ge 1, \iota \ge 0 \end{cases}, \tag{A7 d}$$

$$[\Xi]_{ml\iota}^{2,4} = \sum_{m=0}^{\hat{M}} \int_{-d}^{-h_1} \sum_{l=0}^{\hat{L}} Z_l(k_l z) \sum_{\iota=0}^{\hat{L}} V_\iota(\kappa_\iota z) \mathrm{d}z, \quad m \ge 0, l \ge 0, \iota \ge 0 \quad , \tag{A7 e}$$

$$[\Xi]_{ml\iota}^{2,7} = \begin{cases} 0, & m = 0, l = 0, \iota \ge 0 \\ \sum_{m=1}^{\hat{M}} \int_{-d}^{-h_1} V_0(\kappa_0 z) \sum_{\iota=0}^{\hat{L}} V_\iota(\kappa_\iota z) \, \mathrm{d}z, & m \ge 1, l = 0, \iota \ge 0, \\ \sum_{m=0}^{\hat{M}} \int_{-d}^{-h_1} \sum_{l=1}^{\hat{L}} V_l(\kappa_l z) \sum_{\iota=0}^{\hat{L}} V_\iota(\kappa_\iota z) \, \mathrm{d}z, & m \ge 0, l \ge 1, \iota \ge 0 \end{cases} \tag{A7 f}$$

$$[\Xi]_{ml\iota}^{3,1} = \begin{cases} \sum_{m=0}^{\hat{M}} \int_{-d}^{0} k_0 \mathrm{H}_m^{(1)\prime}(k_0 a) Z_0(k_0 z) \sum_{\iota=0}^{\hat{L}} Z_\iota\left(k_\iota z\right) \mathrm{d}z, & m \ge 0, l = 0, \iota \ge 0 \\ \sum_{m=0}^{\hat{M}} \int_{-d}^{0} \sum_{l=1}^{\hat{L}} k_l \, \mathrm{K}_m^{'}(k_l a) Z_l(k_l z) \sum_{\iota=0}^{\hat{L}} Z_\iota\left(k_\iota z\right) \mathrm{d}z, & m \ge 0, l \ge 1, \iota \ge 0 \end{cases}, \tag{A7 g}$$

$$[\Xi]_{ml\iota}^{3,2}=\begin{cases}\displaystyle\sum_{m=0}^{\hat{M}}\int_{-h_1}^{0}\lambda_0 \mathrm{J}_m^{'}(\lambda_0 a)Y_0(\lambda_0 z)\sum_{\iota=0}^{\hat{L}}Z_\iota\left(k_\iota z\right)\mathrm{d}\,z, & m\geq 0,\, l=0,\ \iota\geq 0\\ \displaystyle\sum_{m=0}^{\hat{M}}\int_{-h_1}^{0}\sum_{l=1}^{\hat{L}}\frac{\lambda_i \mathrm{I}_m^{'}(\lambda_l a)}{\mathrm{I}_m(\lambda_l a)}Y_l(\lambda_l z)\sum_{\iota=0}^{\hat{L}}Z_\iota\left(k_\iota z\right)\mathrm{d}\,z, & m\geq 0,\, l\geq 1,\ \iota\geq 0\end{cases}, \tag{A7 h}$$

$$[\Xi]_{ml\iota}^{3,3}=\sum_{m=0}^{\hat{M}}\sum_{l=0}^{\hat{L}}\left[\beta_{ml}\mathrm{J}_m^{'}(\beta_{ml}a)+D_{ml}^{(1)}\beta_{ml}\mathrm{Y}_m^{'}(\beta_{ml}a)\right]\int_{-h_1}^{0}\frac{\cosh\beta_{ml}z+\dfrac{\omega^2}{g\beta_{ml}}\sinh\beta_{ml}z}{\left(\dfrac{\omega^2}{g}-\beta_{ml}\tanh\beta_{ml}h_1\right)\cosh\left(\beta_{ml}h_1\right)}\sum_{\iota=0}^{\hat{L}}Z_\iota\left(k_\iota z\right)dz, \quad , \tag{A7 i}$$

$m\geq 0, l\geq 0,\ \iota\geq 0$

$$[\Xi]_{ml\iota}^{3,4}=\begin{cases}0, & m=0,\, l=0,\ \iota\geq 0\\ \displaystyle\sum_{m=1}^{\hat{M}}\left(\frac{m}{a}\right)\int_{-d}^{-h_1}V_0(\kappa_0 z)\sum_{\iota=0}^{\hat{L}}Z_\iota\left(k_\iota z\right)\mathrm{d}\,z, & m\geq 1,\, l=0,\ \iota\geq 0\\ \displaystyle\sum_{m=0}^{\hat{M}}\int_{-d}^{-h_1}\sum_{l=1}^{\hat{L}}\frac{\kappa_l \mathrm{I}_m^{'}(\kappa_l a)}{\mathrm{I}_m(\kappa_l a)}V_l(\kappa_l z)\sum_{\iota=0}^{\hat{L}}Z_\iota\left(k_\iota z\right)\mathrm{d}\,z, & m\geq 0,\, l\geq 1,\ \iota\geq 0\end{cases}, \tag{A7 j}$$

$$[\Xi]_{ml\iota}^{3,5}=\sum_{m=0}^{\hat{M}}\sum_{l=0}^{\hat{L}}\left[\beta_{ml}\mathrm{J}_m^{'}(\beta_{ml}a)+D_{ml}^{(2)}\beta_{ml}\mathrm{Y}_m^{'}(\beta_{ml}a)\right]\int_{-d}^{-h_1}\frac{\cosh\beta_{mi}\left(z+d\right)}{\beta_{mi}\tanh\beta_{mi}h_2\cosh\beta_{mi}h_2}\sum_{\iota=0}^{\hat{L}}Z_\iota\left(k_\iota z\right)dz, \quad , \tag{A7 k}$$

$m\geq 0, l\geq 0,\ \iota\geq 0$

$$[\Xi]_{ml\iota}^{3,6}=\begin{cases}\displaystyle\sum_{m=0}^{\hat{M}}\lambda_0 \mathrm{Y}_m^{'}(\lambda_0 a)\int_{-h_1}^{0}Y_0(\lambda_0 z)\sum_{\iota=0}^{\hat{L}}Z_\iota\left(k_\iota z\right)\mathrm{d}\,z, & m\geq 0,\, l=0,\ \iota\geq 0\\ \displaystyle\sum_{m=0}^{\hat{M}}\int_{-h_1}^{0}\sum_{l=1}^{\hat{L}}\frac{\lambda_i \mathrm{K}_m^{'}(\lambda_l a)}{\mathrm{K}_m(\lambda_l a)}Y_l(\lambda_l z)\sum_{\iota=0}^{\hat{L}}Z_\iota\left(k_\iota z\right)\mathrm{d}\,z, & m\geq 0,\, l\geq 1,\ \iota\geq 0\end{cases}, \tag{A7 l}$$

$$[\Xi]_{ml\iota}^{3,7}=\begin{cases}\displaystyle\frac{1}{a}\int_{-d}^{-h_1}V_0(\kappa_0 z)\sum_{\iota=0}^{\hat{L}}Z_\iota\left(k_\iota z\right)dz, & m=0,\, l=0,\ \iota\geq 0\\ \displaystyle\sum_{m=1}^{\hat{M}}\left(-\frac{m}{a}\right)\int_{-d}^{-h_1}V_0(\kappa_0 z)\sum_{\iota=0}^{\hat{L}}Z_\iota\left(k_\iota z\right)\mathrm{d}\,z, & m\geq 1,\, l=0,\ \iota\geq 0\\ \displaystyle\sum_{m=0}^{\hat{M}}\int_{-d}^{-h_1}\sum_{l=1}^{\hat{L}}\frac{\kappa_l \mathrm{K}_0^{'}(\kappa_l a)}{\mathrm{K}_0(\kappa_l a)}V_l(\kappa_l z)\sum_{\iota=0}^{\hat{L}}Z_\iota\left(k_\iota z\right)\mathrm{d}\,z, & m\geq 0,\, l\geq 1,\ \iota\geq 0\end{cases}, \tag{A7 m}$$

$$[\Xi]_{ml\iota}^{4,2}=\begin{cases}\displaystyle\sum_{m=0}^{\hat{M}}-\mathrm{i}kGY_0(-\lambda_0 h_1)\int_b^a \mathrm{J}_m(\lambda_0 r)\sum_{\iota=0}^{\hat{L}}\mathrm{J}_m\left(\beta_{m\iota}r\right)rdr, & m\geq 0,\, l=0,\ \iota\geq 0\\ \displaystyle\sum_{m=0}^{\hat{M}}\sum_{l=1}^{\hat{L}}-\mathrm{i}kGY_l(-\lambda_l h_1)\int_b^a\frac{\mathrm{I}_m(\lambda_l r)}{\mathrm{I}_m(\lambda_l a)}\sum_{\iota=0}^{\hat{L}}\mathrm{J}_m\left(\beta_{m\iota}r\right)rdr, & m\geq 0,\, l\geq 1,\ \iota\geq 0\end{cases}, \tag{A7 n}$$

$$[\Xi]_{ml\iota}^{4,3}=\sum_{m=0}^{\hat{M}}\sum_{l=0}^{\hat{L}}\left[1+\mathrm{i}kG\frac{1-\dfrac{\omega^2}{g\beta_{ml}}\tanh\left(\beta_{ml}h_1\right)}{\left(\dfrac{\omega^2}{g}-\beta_{ml}\tanh\beta_{ml}h_1\right)}\right]\int_b^a\left[\mathrm{J}_m(\beta_{ml}r)+D_{ml}^{(1)}\mathrm{Y}_m(\beta_{ml}r)\right]\sum_{\iota=0}^{\hat{L}}\mathrm{J}_m\left(\beta_{m\iota}r\right)\mathrm{r}dr, \quad , \tag{A7 o}$$

$m\geq 0, l\geq 0,\ \iota\geq 0$

$$[\Xi]_{ml\iota}^{4,4}=\begin{cases}\mathrm{i}kGV_0(-\kappa_0h_1)\int_b^a\sum_{\iota=0}^{\hat{L}}\mathrm{J}_m\left(\beta_{m\iota}r\right)rdr, & m=0,\ l=0,\ \iota\geq 0\\ \sum_{m=1}^{\hat{M}}\mathrm{i}kGV_0(-\kappa_0h_1)\int_b^a\left(\frac{r}{a}\right)^m\sum_{\iota=0}^{\hat{L}}\mathrm{J}_m\left(\beta_{m\iota}r\right)rdr, & m\geq 1,\ l=0,\ \iota\geq 0\\ \sum_{m=0}^{\hat{M}}\sum_{l=1}^{\hat{L}}\mathrm{i}kGV_l(-\kappa_lh_1)\int_b^a\frac{\mathrm{I}_m(\kappa_lr)}{\mathrm{I}_m(\kappa_la)}\sum_{\iota=0}^{\hat{L}}\mathrm{J}_m\left(\beta_{m\iota}r\right)rdr, & m\geq 1,\ l=0,\ \iota\geq 0\end{cases},\qquad \text{(A7 p)}$$

$$[\Xi]_{ml\iota}^{4,5}=\sum_{m=0}^{\hat{M}}\sum_{l=0}^{\hat{L}}\mathrm{i}kG\frac{1}{\beta_{ml}\tanh\beta_{ml}h_2}\int_b^a\left[\mathrm{J}_m(\beta_{ml}r)+D_{ml}^{(2)}\mathrm{Y}_m(\beta_{ml}r)\right]\sum_{\iota=0}^{\hat{L}}\mathrm{J}_m\left(\beta_{m\iota}r\right)\mathrm{r}dr,\ ,\qquad \text{(A7 q)}$$

$m\geq 0,\ l\geq 0,\ \iota\geq 0$

$$[\Xi]_{ml\iota}^{4,6}=\begin{cases}\sum_{m=0}^{\hat{M}}-\mathrm{i}kGY_0(-\lambda_0h_1)\int_b^a\mathrm{Y}_m(\lambda_0r)\sum_{\iota=0}^{\hat{L}}\mathrm{J}_m\left(\beta_{m\iota}r\right)rdr, & m\geq 0,\ l=0,\ \iota\geq 0\\ \sum_{m=0}^{\hat{M}}\sum_{l=1}^{\hat{L}}-\mathrm{i}kGY_l(-\lambda_lh_1)\int_b^a\frac{\mathrm{K}_m(\lambda_lr)}{\mathrm{K}_m(\lambda_la)}\sum_{\iota=0}^{\hat{L}}\mathrm{J}_m\left(\beta_{m\iota}r\right)rdr, & m\geq 0,\ l\geq 1,\ \iota\geq 0\end{cases},\qquad \text{(A7 r)}$$

$$[\Xi]_{ml\iota}^{4,7}=\begin{cases}\mathrm{i}kGV_0(-\kappa_0h_1)\int_b^a\ln\left(\frac{r}{a}\right)\sum_{\iota=0}^{\hat{L}}\mathrm{J}_m\left(\beta_{m\iota}r\right)rdr, & m=0,\ l=0,\ \iota\geq 0\\ \sum_{m=1}^{\hat{M}}\mathrm{i}kGV_0(-\kappa_0h_1)\int_b^a\left(\frac{r}{a}\right)^{-m}\sum_{\iota=0}^{\hat{L}}\mathrm{J}_m\left(\beta_{m\iota}r\right)rdr, & m\geq 1,\ l=0,\ \iota\geq 0\\ \sum_{m=0}^{\hat{M}}\sum_{l=1}^{\hat{L}}\mathrm{i}kGV_l(-\kappa_lh_1)\int_b^a\frac{\mathrm{K}_0(\kappa_lr)}{\mathrm{K}_0(\kappa_la)}\sum_{\iota=0}^{\hat{L}}\mathrm{J}_m\left(\beta_{m\iota}r\right)rdr, & m\geq 0,\ l\geq 1,\ \iota\geq 0\end{cases},\qquad \text{(A7 s)}$$

$$[\Xi]_{ml\iota}^{5,3}=\sum_{m=0}^{\hat{M}}\int_b^a\sum_{l=0}^{\hat{L}}\left[\mathrm{J}_m(\beta_{ml}r)+D_{ml}^{(1)}\mathrm{Y}_m(\beta_{ml}r)\right]\sum_{\iota=0}^{\hat{L}}\mathrm{J}_m\left(\beta_{m\iota}r\right)rdr,\quad m\geq 0,\ l\geq 0,\ \iota\geq 0,\qquad \text{(A7 t)}$$

$$[\Xi]_{ml\iota}^{5,5}=\sum_{m=0}^{\hat{M}}\int_b^a\sum_{l=0}^{\hat{L}}\left[\mathrm{J}_m(\beta_{ml}r)+D_{ml}^{(2)}\mathrm{Y}_m(\beta_{ml}r)\right]\sum_{\iota=0}^{\hat{L}}\mathrm{J}_m\left(\beta_{m\iota}r\right)rdr,\quad m\geq 0,\ l\geq 0,\ \iota\geq 0,\qquad \text{(A7 u)}$$

$$[\Xi]_{ml\iota}^{6,2}=\begin{cases}\sum_{m=0}^{\hat{M}}\lambda_0\mathrm{J}_m^{'}(\lambda_0b)\int_{-h_1}^{-0}Y_0(\lambda_0z)\sum_{\iota=0}^{\hat{L}}Y_\iota\left(\lambda_\iota z\right)dz, & m\geq 0,\ l=0,\ \iota\geq 0\\ \sum_{m=0}^{\hat{M}}\sum_{l=1}^{\hat{L}}\frac{\lambda_l\mathrm{I}_m^{'}(\lambda_lb)}{\mathrm{I}_m(\lambda_la)}\int_{-h_1}^{-0}Y_l(\lambda_lz)\sum_{\iota=0}^{\hat{L}}Y_\iota\left(\lambda_\iota z\right)dz, & m\geq 0,\ l\geq 1,\ \iota\geq 0\end{cases},\qquad \text{(A7 v)}$$

$$[\Xi]_{ml\iota}^{6,3}=\sum_{m=0}^{\hat{M}}\sum_{l=0}^{\hat{L}}\left[\beta_{ml}\mathrm{J}_m^{'}(\beta_{ml}b)+D_{ml}^{(1)}\beta_{ml}\mathrm{Y}_m^{'}(\beta_{ml}b)\right]\int_{-h_1}^{-0}\frac{\cosh\beta_{ml}z+\dfrac{\omega^2}{g\beta_{ml}}\sinh\beta_{ml}z}{\left(\dfrac{\omega^2}{g}-\beta_{ml}\tanh\beta_{ml}h_1\right)\cosh\left(\beta_{ml}h_1\right)}\sum_{\iota=0}^{\hat{L}}Y_\iota\left(\lambda_\iota z\right)dz,\ ,\qquad \text{(A7 w)}$$

$m\geq 0,\ l\geq 0,\ \iota\geq 0$

$$[\Xi]_{ml\iota}^{6,6}=\begin{cases}\sum_{m=0}^{\hat{M}}\lambda_0\mathrm{Y}_m^{'}(\lambda_0b)\int_{-h_1}^{-0}Y_0(\lambda_0z)\sum_{\iota=0}^{\hat{L}}Y_\iota\left(\lambda_\iota z\right)dz, & m\geq 0,\ l=0,\ \iota\geq 0\\ \sum_{m=0}^{\hat{M}}\sum_{l=1}^{\hat{L}}\frac{\lambda_l\mathrm{K}_m^{'}(\lambda_lb)}{\mathrm{K}_m(\lambda_la)}\int_{-h_1}^{-0}Y_l(\lambda_lz)\sum_{\iota=0}^{\hat{L}}Y_\iota\left(\lambda_\iota z\right)dz, & m\geq 0,\ l\geq 1,\ \iota\geq 0\end{cases},\qquad \text{(A7 x)}$$

$$[\Xi]^{7,4}_{ml\iota}=\begin{cases}0, & m=0,\, l=0,\, \iota\ge 0\\ \sum_{m=1}^{\hat{M}}\dfrac{mb^{m-1}}{a^{m}}\int_{-d}^{-h_1}V_0(\kappa_0 z)\sum_{\iota=0}^{\hat{L}}V_\iota(\kappa_\iota z)\,\mathrm{d}\,z, & m\ge 1,\, l=0,\, \iota\ge 0\\ \sum_{m=0}^{\hat{M}}\int_{-d}^{-h_1}\sum_{l=1}^{\hat{L}}\dfrac{\kappa_l \mathrm{I}'_m(\kappa_l b)}{\mathrm{I}_m(\kappa_l a)}V_l(\kappa_l z)\sum_{\iota=0}^{\hat{L}}V_\iota(\kappa_\iota z)\,\mathrm{d}\,z, & m\ge 0,\, l\ge 1,\, \iota\ge 0\end{cases}, \tag{A7 y}$$

$$[\Xi]^{7,5}_{ml\iota}=\sum_{m=0}^{\hat{M}}\sum_{l=0}^{\hat{L}}\left[\beta_{ml}\mathrm{J}'_m(\beta_{ml}b)+D^{(2)}_{ml}\beta_{ml}\mathrm{Y}'_m(\beta_{ml}b)\right]\int_{-d}^{-h_1}\frac{\cosh\beta_{ml}\left(z+d\right)}{\beta_{ml}\tanh\beta_{ml}h_2\cosh\beta_{ml}h_2}\sum_{\iota=0}^{\hat{L}}V_\iota(\kappa_\iota z)dz, \quad , \tag{A7 z}$$

$m\ge 0,\, l\ge 0,\, \iota\ge 0$

and

$$[\Xi]^{7,7}_{ml\iota}=\begin{cases}\dfrac{1}{b}\int_{-d}^{-h_1}V_0(\kappa_0 z)\sum_{\iota=0}^{\hat{L}}V_\iota(\kappa_\iota z)\,\mathrm{d}\,z, & m=0,\, l=0,\, \iota\ge 0\\ \sum_{m=1}^{\hat{M}}\dfrac{-mb^{-m-1}}{a^{-m}}\int_{-d}^{-h_1}V_0(\kappa_0 z)\sum_{\iota=0}^{\hat{L}}V_\iota(\kappa_\iota z)\,\mathrm{d}\,z, & m\ge 1,\, l=0,\, \iota\ge 0\\ \sum_{m=0}^{\hat{M}}\int_{-d}^{-h_1}\sum_{l=1}^{\hat{L}}\dfrac{\kappa_l \mathrm{K}'_m(\kappa_l b)}{\mathrm{K}_m(\kappa_l a)}V_l(\kappa_l z)\sum_{\iota=0}^{\hat{L}}V_\iota(\kappa_\iota z)\,\mathrm{d}\,z, & m\ge 0,\, l\ge 1,\, \iota\ge 0\end{cases}. \tag{A7 z1}$$

Considering the radiational problem caused by the heave motion of the vertical cylinder with a submerged porous plate, on the common boundaries between different sub-regions, the radiational velocity potentials must satisfy appropriate transmission conditions:

$$\begin{cases}\dfrac{\partial\phi_1}{\partial r}=\dfrac{\partial\left(\phi_{2,v}+\phi_{2,h}\right)}{\partial r} & \text{for } -h_1<z<0,\ r=a\\ \dfrac{\partial\phi_1}{\partial r}=\dfrac{\partial\left(\phi_{3,v}+\phi_{3,h}\right)}{\partial r} & \text{for } -d<z<-h_1,\ r=a\\ \dfrac{\partial\phi_{2,h}}{\partial z}=\dfrac{\partial\phi_{3,h}}{\partial z} & \text{for } b<r<a,\ z=-h_1\\ \dfrac{\partial\left(\phi_{2,v}+\phi_{2,h}\right)}{\partial r}=0 & \text{for } -h_1<z<0,\ r=b\\ \dfrac{\partial\left(\phi_{3,v}+\phi_{3,h}\right)}{\partial r}=0 & \text{for } -d<z<-h_1,\ r=b\end{cases}, \tag{A8}$$

and

$$\begin{cases}\phi_1=\phi_{2,v} & \text{for } -h_1<z<0,\ r=a\\ \dfrac{\partial\phi_{2,h}}{\partial z}=1+\mathrm{i}k_0G\left(\phi_{3,v}+\phi_{3,h}-\phi_{2,v}-\phi_{2,h}\right) & \text{for } b<r<a,\ z=-h_1\\ \phi_1=\phi_{3,v} & \text{for } -d<z<-h_1,\ r=a\end{cases}. \tag{A9}$$

We obtain the set of algebraic equations by using the orthogonal relationship of the vertical, radial, and circular eigenfunctions, which is similar to the solving process of the diffraction problem. Thus, the radiational velocity potentials in relevant sub-regions can be determined accurately.

References:

Dhanak, M.R., Xiros, N.I. (Eds.), 2016. Springer Handbook of Ocean Engineering. Springer International Publishing, Cham.

Takahashi, S., et al. PERFORMANCE EVALUATION of PERFORATED-WALL CAISSONS by VOF NUMERICAL SIMULATIONS. in Proceedings of the Coastal Engineering Conference. 2003.

Huang, Z., Y. Li and Y. Liu, Hydraulic performance and wave loadings of perforated/slotted coastal structures: A review. Ocean Engineering, 2011. 38(10): p. 1031-1053.

Liu, Y. and H.J. Li, Wave reflection and transmission by porous breakwaters: A new analytical solution. Coastal Engineering, 2013. 78: p. 46-52.

Mackay E, Johanning L. Comparison of analytical and numerical solutions for wave interaction with a vertical porous barrier. Ocean Engineering, 2020, 199: p. 107032.

Zhai, Z., et al., Semi-analytical solution of cnoidal wave diffraction around a double-layer arc-shaped vertical porous breakwater. Journal of Fluids and Structures, 2021. 103: p. 103261.

Zheng, S.M., Meylan, M.H., Greaves, D., Iglesias, G., Water-wave interaction with submerged porous elastic disks. Physics of Fluids, 2020, 32, p. 047106.

Sun, C. and V. Jahangiri, Mitigation of monopile offshore wind turbines under wind and wave loading. Americas Conference on Wind Engineering, 2017.

Kaligatla, R.B., Manisha, Sahoo, T., Wave trapping by dual porous barriers near a wall in the presence of bottom undulation. J. Marine. Sci. Appl., 2017, 16, p. 286–297.

Koley, S., Sahoo, T., Integral equation technique for water wave interaction by an array of vertical flexible porous wave barriers. ZAMM - Journal of Applied Mathematics and Mechanics / Zeitschrift für Angewandte Mathematik und Mechanik 101, 2021.

Chanda, A., Nandan Bora, S., Effect of a porous sea-bed on water wave scattering by two thin vertical submerged porous plates. European Journal of Mechanics - B/Fluids, 2020, 84, p. 250–261.

Chanda, A., Nandan Bora, S., Scattering of Flexural Gravity Waves by a Pair of Submerged Vertical Porous Barriers Located Above a Porous Sea-Bed. Journal of Offshore Mechanics and Arctic Engineering, 2022, 144, p. 011201.

Williams, A.N., W. Li and K.H. Wang, Water wave interaction with a floating porous cylinder. Ocean Engineering, 2000. 27(1): p. 1-28.

Teng, B., Han, L., Li Y.C., Ware diffraction from a vertical cylinder with two uniform columns and porous outer wall. China Ocean Engineering, 2000, 14(3), p. 297-306.

Teng, B., Zhao, M., Li, Y.C., Wave diffraction from a cylinder with porous upper wall and an inner column. Acta Oceanologica Sinica, 2001, 23(6), p. 133-142.

Sun, L., et al., Wave action on structures of combined cylinders. China Ocean Engineering, 2005. 19(3): p. 375-384.

Ning, D.Z., et al., Wave diffraction from a truncated cylinder with an upper porous sidewall and an inner column. Ocean Engineering, 2017. 130: p. 471-481.

Liang, H., et al., Efficient methods free of irregular frequencies in wave and solid/porous structure interactions. Journal of Fluids and Structures, 2020. 98.

Mackay, E.B.L., et al. Verification of a boundary element model for wave forces on structures with porous elements. in Advances in Renewable Energies Offshore - Proceedings of the 3rd International Conference on Renewable Energies Offshore, RENEW 2018. 2019.

Mackay E, Liang H, Johanning L. A BEM model for wave forces on structures with thin porous elements. Journal of Fluids and Structures, 2021, 102: 103246.

Sarkar, A. and S.N. Bora, Hydrodynamic forces due to water wave interaction with a bottom-mounted surface-piercing compound porous cylinder. Ocean Engineering, 2019. 171: p. 59-70.

Sarkar, A. and S.N. Bora, Hydrodynamic forces and moments due to interaction of linear water waves with truncated partial-porous cylinders in finite depth. Journal of Fluids and Structures, 2020. 94: p. 102898.

Liu, H., et al., Wave diffraction by vertical cylinder with multiple concentric perforated walls. Ocean Engineering, 2018. 166: p. 242-252.

Behera, H., Gayathri, R., Selvan, S.A., Wave Attenuation by Multiple Outer Porous Barriers in the Presence of an Inner Rigid Cylinder. J. Waterway, Port, Coastal, Ocean Eng, 2020, 146, p. 04019035.

Wu, J. and A.T. Chwang, Wave diffraction by a vertical cylinder with a porous ring plate. Journal of Engineering Mechanics, 2002. 128(2): p. 164-171.

Liu, Y., et al., A new approximate analytic solution for water wave scattering by a submerged horizontal porous disk. Applied Ocean Research, 2011. 33(4): p. 286-296.

Chwang A T, Wu J. Wave scattering by submerged porous disk. Journal of engineering mechanics, 1994, 120(12), p. 2575-2587.

Sollitt, C.K., Cross, R.H., Wave transmission through permeable breakwaters. In: Proceedings of 13th International Conference Coastal Engineering, ASCE, New York, 1972, p. 1847-1865.

Yu, X.P., Diffraction of water waves by porous breakwaters. J. Waterway, Port, Coastal Ocean Eng, 1995, 121(6), p. 275-282.

Martin P A, Farina L. Radiation of water waves by a heaving submerged horizontal disc. Journal of Fluid Mechanics, 1997, 337(4), p. 365-379.

Zhao F, Zhang T, Wan R, et al. Hydrodynamic loads acting on a circular porous plate horizontally submerged in waves. Ocean Engineering, 2017, 136, p. 168-177.

Li Y., Zhao X.L., Geng J.. Analytical analysis of sway mode problem of the vertical cylinder with a submerged plate. CHINESE OCEAN ENGINEERING SOCIETY, Proceedings of the 20th Chinese Ocean (Shore) Engineering Symposium, 2022.

Tromans S, P, Anaturk R, A, Hagemeijer, P.. A new model for the kinematics of large ocean waves-application as a design wave. The first international offshore and polar engineering conference, 1991.